Journal of Sailing Technology 2025, volume 10, issue 1, pp. 279 – 313.
The Society of Naval Architects and Marine Engineers.

Keel Concept for Modern Wind-Assisted Commercial Ships based on the Vortex-Lift Principle

Siegfried Wagner
Fraunhofer WG Sustainable Maritime Mobility, Emden/Leer University of Applied Sciences, Germany, siegfried.wagner@hs-emden-leer.de

Sascha Strasser
Fraunhofer WG Sustainable Maritime Mobility, Emden/Leer University of Applied Sciences, Germany.

Michael Vahs
Fraunhofer WG Sustainable Maritime Mobility, Emden/Leer University of Applied Sciences, Germany.

Manuscript received June 24, 2025; revision received August 28, 2025; accepted September 08, 2025.

Abstract. Commercial vessels powered by large wind propulsion systems experience not only thrust but also considerable side-force and yawing moments that must be equalized by the hydrodynamic layout and design of the vessel. Modern racing yachts handle this issue by the usage of large asymmetric daggerboards or foils while traditional sailing vessels rely mainly on centered bar-keels in combination with deadrise and keel-rake. The goal of every hydrodynamic concept for vessels powered by wind is to provide a system that equalizes cross-force and yawing moment while added resistance is kept as low as possible for maximizing the benefit from the wind propulsion system. This paper presents the development and analysis of a special kind of bilge-keel system (Wagner-Keels) that is suitable for modern ship hull geometries that are restricted by draft limitations and aiming at a cost-efficient solution for tackling the requirements of large wind propulsion system used for primary ship propulsion. The novel approach, compared to existing concepts, is the delta-shaped planform of these bilge-keels, aiming at maximizing vortex-lift effects that are created due to the triangular shape of the keels (vortex-lift principle). Research, based on CFD-RANSE methods as well as towing-tank analysis, was done at Hamburg University of Technology (TUHH) in 2015 and in the framework of the project ‘Transitioning to Low Carbon Sea Transport’ (LCST) at ‘University of Applied Science Emden/Leer’ (HEL) in 2022 for the development of the concept design of the primarily wind powered island supply vessel JUREN-AE, operating in the Republic of Marshall Islands since July 2024. The research focus lies on hydrodynamic performance of this novel keel design concept, compared to alternative design solutions with respect to optimized sailing capabilities. The benefit of reduced total drag and increased force-ratios of this novel concept could be shown for modern flat-bottom hull forms (commercial trading vessels) as well as for hull-forms designed with deadrise (traditional sailing vessels). Further the beneficial behavior of the concept concerning heeling due to wind force as well as its positive influence on the positioning of the hydrodynamic center of effort in line with the requirements of the wind propulsion system was analyzed in detail.

Keywords: Hydrodynamics, Bilge-Keels, Vortex-Lift, Wagner-Keels, Primary Wind Propulsion, Ship Efficiency, Low Carbon Sea Transport

NOMENCLATURE

1+k	Form Factor [-]
A_{lat}	Lateral Area [m²]
A_R	Aspect-Ratio [-]
C_A	Aerodynamic cross-force [N]
C_A/D_A	Aerodynamic 'force-ratio' [-]
C_C	Cross-force coefficient, equals lift-force coefficient C_L [-]
C_D	Drag-force coefficient [-]
$C_{E,aero}$	Aerodynamic center of effort [x/L_{pp}]
$C_{E,hull}$	Center of effort for ship hull [x/L_{pp}]
$C_{E,hydro}$	Hydrodynamic center of effort [x/L_{pp}]
$C_{E,keel}$	Center of effort for keel system [x/L_{pp}]
$C_{E,rudder}$	Center of effort for rudder [x/L_{pp}]
C_H	Hydrodynamic cross-force [N]
C_H/D_H	Hydrodynamic force-ratio [-]
C_L	Lift force coefficient [-]
C_r	Residuary resistance coefficient [-]
C_t	Total resistance coefficient [-]
$C_{x,vh}$	Coefficient of force in direction of vessel motion (equals $-C_D$) [-]
$C_{xy,vh}$	force coefficient induced by cross-force (equals the negative induced drag) [-]
$C_{y,vh}$	force coefficient perpendicular to direction of vessel motion (equals C_L) [-]
D_A	Aerodynamic drag-force [N]
D_H	Hydrodynamic drag-force [N]
Fn	Froude number [-]
F_x	Force in x-direction of ship coordinate system [N]
$F_{x,vh}$	Force in direction of vessel motion [N]
$F_{xy,vh}$	Equals negative induced drag, caused by cross-force [N]
F_y	Force in y-direction of ship coordinate system [N]
$F_{y,vh}$	Cross-force, perpendicular to direction of vessel motion [N]
R_t	Total resistance [kN]
S	wetted surface area [m^2]
U_{10}	True wind speed in height of 10 m [m s^{-1}]
U_A	Aerodynamic flow velocity, Apparent wind speed [m s^{-1}]
U_T	True wind speed corrected for height above sea-level [m s^{-1}]
V_h	Hydrodynamic flow velocity, equals negative sailing speed (V_s) [m s^{-1}]
V_S	Sailing speed [m s^{-1}]
w	Wake number [-]
α	Angle of attack for rudder [deg]
β_A	Aerodynamic angle of attack [deg]
β_H	Hydrodynamic angle of attack, Hydrodynamic leeway angle [deg]
δ_{rudder}	Rudder angle [deg]
ε_A	Aerodynamic glide angle [deg]
ε_H	Hydrodynamic glide angle [deg]
γ_A	Apparent wind course through water, angle between air and water flow against ship [deg]
ρ	Fluid density [kg m^{-3}]
AP	Aft Perpendicular
CFD	Computational Fluid Dynamics
CS-v1	Center Skeg design concept variant 1 with standard bilge-keels
DF-v4	Double Fin design concept variant 4 with standard bilge-keels
DOF	Degree Of Freedom
EFD	Experimental Fluid Dynamics

GIZ	Deutsche Gesellschaft für Internationale Zusammenarbeit
HEL	Hochschule Emden/Leer - University of Applied Sciences
IKI	International Climate Initiative
KF	Keel-Rake (German: Kielfall)
LCST	R&D project: transition to low carbon sea transport
RANSE	Reynolds-Averaged Navier-Stokes Equations
RMI	Republic of the Marshall Islands
RoA	Hull without appendages (German: Rumpf ohne Anhänge)
RPM	Revolutions Per Minute
Rw	Isolated forces due to ship-wave system
SBT	Slender-Body-Theory calculation procedure
SK-v4	Large delta-shaped side-keel design variant 4, Wagner-Keels
SK-v7	Small delta-shaped side-keel design variant 7, Wagner-Keels
TUHH	Hamburg University of Technology
WPS	Wind propulsion system

1. INTRODUCTION

The age of sailing ended with the development of modern diesel engines and their introduction to the shipping sector. At the same time hull forms, that have previously been adapted to the requirements of proportionally large wind propulsion systems, changed dramatically to suit the new requirements of main engine and propeller for thrust generation. Furthermore, hull shapes adapted towards specific cargo demands and the challenges and restrictions posed by new trading routes and seaports. Today we have specialized ships, perfectly adapted to modern port infrastructure and specific cargo demands. These ships usually have flat bottom hulls without any dead-rise or keel-rake. Traditionally, sailing vessels mostly relied on a centered bar-keel in combination with a deadrise hull design. Aft trim or keel-rake was used to move the hydrodynamic center of effort further aft to meet the requirements of the wind propulsion system.

These very specific hull design criteria used in combination with wind propulsion systems during the age of sails, are not existent anymore in today's trading fleet. If today's commercial fleet is reintroduced to the concept of primary wind propulsion, new keel concepts for handling large side-forces generated by large wind propulsion systems, need to be developed, adapted to today's hull-shapes. Recent studies (van der Kolk, 2020, 2024) propose standard low aspect -ratio bilge keels, used for damping of rolling motions (Mohsin, 2016) since decades, as an efficient measure for countering side-forces from wind propulsion systems. The standard bilge-keels are usually designed as rectangular profiles with rounded edges.

The topic of this research study is the development and analysis of delta-shaped low aspect-ratio bilge-keel system, based on the principle of vortex lift generation, suitable for modern hulls of nowadays commercial fleet. These delta-shaped bilge-keel concepts are compared to alternative design solutions (double fins and centered-bar-keels) for evaluating the advantages of the novel design approach.

First basic research on the topic was done during a master thesis of one of the authors, whereby a large variety of keel shape variations and concepts was analyzed and compared via CFD-RANSE methods at Hamburg University of Technology (TUHH) . This initial research was continued in the framework of the concept design and scientific research at Emden/Leer University of Applied Sciences (HEL) for the design and building of the primary wind powered sailing cargo ship JUREN-AE in the framework of the IKI funded project 'Transitioning to Low Carbon Sea Transport' (LCST) for the Republic of the Marshall Islands (RMI).

2. PHYSICS OF SAILING – THE EQUILIBRIUM OF FORCES AND MOMENTS

The basis for evaluating the effectiveness of an appendage system for a primary wind propelled vessel is its ability to counteract the forces and moments resulting from the wind-propulsion system. If we assume a large wind propulsion system in relation to the size of the ship, these forces and moments also dominate the design of the ship's hydrodynamic layout.

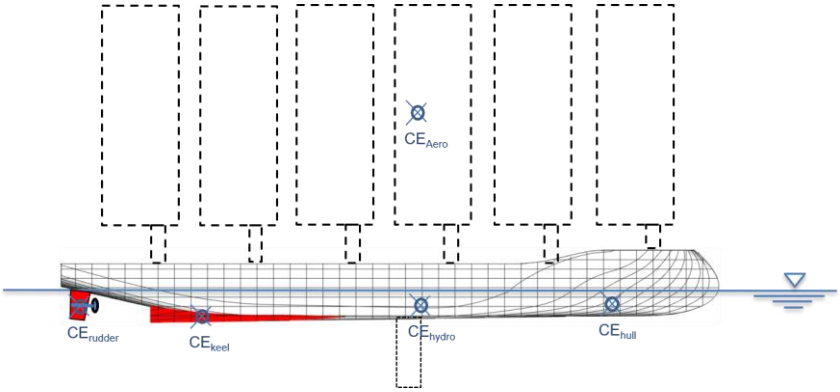

Figure 1. Aero- and hydrodynamic layout for a primary wind propelled ship.

For sailing a straight course, all forces and moments need to be in perfect balance. To reach this balance the hydrodynamic layout must be adapted towards the aerodynamic requirements. Since the natural center of effort for most modern hulls ($C_{E,hull}$) is positioned somewhere near to the bow, the rudder would need to create a large side-force, in order to align the 'hydrodynamic center of effort' ($C_{E,hydro}$) to the 'aerodynamic center of effort' ($C_{E,aero}$).

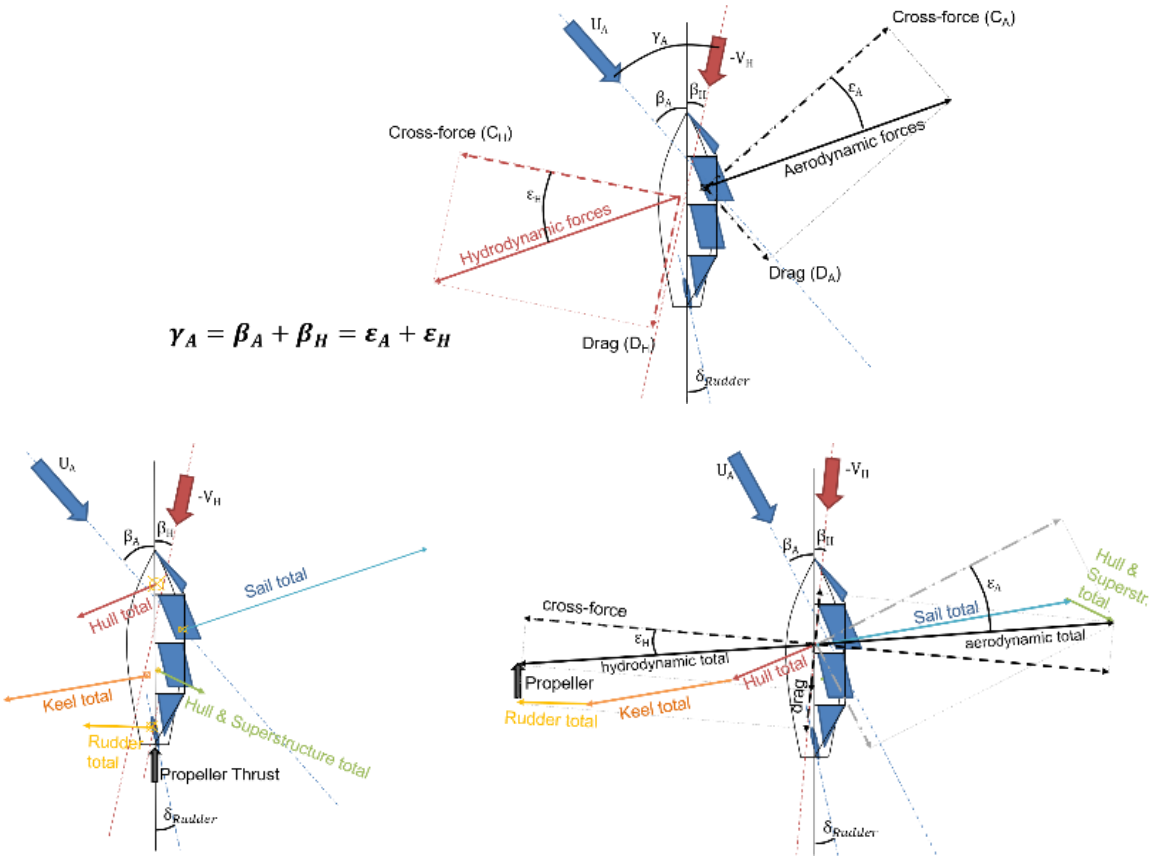

Figure 2. Equilibrium of forces and moments for a sailing ship.

Even though, the rudder is a very effective device for generating side-forces and should therefore be considered in the overall hydrodynamic concept, it is clear that the capabilities of the rudder are limited by its relatively small size. Further, the rudder is still needed for maneuvering of the 'sailing' ship as well. Stationary rudder angles of more than five degrees for balancing the ship on a straight course should be avoided. Therefore, an efficient keel system is needed to prevent overloading of the rudder and to increase total side-force capabilities of the hydrodynamic layout of the vessel. Efficiency of the hydrodynamic system is defined by the 'glide-angle' (γ_A) or 'force-ratio' (Schenzle, 2010). The higher the force-ratio, the better the sailing characteristics of the ship will be, expressed by smaller angles sailed towards the apparent wind. A large keel system will however also increase the initial drag of the vessel, while sailing in engine mode or downwind where only little side-force is required. The longitudinal positioning of the keel system gives control over the $C_{E,hydro}$ while its size defines the effective leeway angle as well as initial drag of the ship.

3. INITIAL INVESTIGATIONS AT TUHH

In the framework of two research studies the concept of vortex-lift as a means for the generation of hydrodynamic cross-force (lift) was analyzed. In 2011 a first CFD-RANSE based work was done at TUHH to analyze vortex-lift effects at the raked keels of traditional sailing vessels (Wagner, 2011). The concept of vortex-lift was then picked up again in 2014 (Wagner, 2015) for further investigations in the context of sideward positioned keels for large commercial vessels. Focus of this paper lies on this second scientific research work, which basically represents a large shape variation study on different delta-shaped side-keels. Variations were done in size, position, angle and leading-edge contour. The different delta shaped side-keels were compared towards two alternate keel design concepts, that fulfil the same basic requirements. All appendage variations were attached towards a standard hull (hull without skeg). Apart from cross-force, drag and yawing moment, emphasis was given to analyze the behavior of the different appendage concepts for changing heeling angles and effects caused by keel-rake (aft trim) on the yawing moment. Based on a CFD-RANSE calculation approach, the study also provides detailed insights into flow conditions as well as force and pressure distributions for the different appendage systems.

3.1 Concept development

Usually lift (cross-force for sailing ships) is generated by a profiled wing or foil. The higher the aspect ratio of this wing, the lower is the additional induced drag, resulting in high force-ratios and minimized leeway angles. Additionally, to the technical challenges of a deep retractable wing that is used to counter the side forces of a commercial ship, operation and maintenance costs pose significant economic challenge for a concept aiming at economic efficiency for cargo transportation. Instead of conventional means of lift generation by the use of a profiled foil, the proposed fixed keel concept builds on the idea of using low aspect-ratio delta-wings that rely on vortex-lift capabilities, similar to the delta-wings that are used for high speed airplanes (Polhamus, 1966, Luckering, 2019), to overcome the difficulties concerning draft limitations or additional high expanses for sophisticated technical solutions.

3.1.1 The Principle of Vortex-Lift

The concept of vortex lift on a delta wing basically maximizes the tip vortex of the wing and guides this vortex along the slanted leading edge of the wing. The lift is generated by the negative pressure field within this vortex in addition to the potential lift of the surrounding flow (Polhamus, 1966). Experiments with this kind of wing show that this vortex is not only adding to the generated lift but also affects the boundary layer separation that usually causes the stall of the flow around a conventional profile (Marchaj, 2003). Stall leads to drastic reduction in the generated lift or side force. For delta wings however, this phenomenon cannot be observed. The lift coefficient for a delta wing reaches its maximum at a high angle of attack of 40° to 60° depending on its planform (Marchaj, 2003). Further increase of the inflow angle will not result in a sudden drop in the generated forces

but will gradually transit into the typically separated flow conditions. The reason for this gradual change of forces is likely the accelerated flow inside the attached vortex that prevents the formation of a detachment bubble by a steady downstream transport inside the vortex core. For conventional wings the formation of a detachment bubble ultimately leads to stall and breakdown of the cross-force (lift) generation (Marchaj, 2003). Another important characteristic of a low aspect-ratio delta-wing is the comparatively low resistance coefficient at small angles of attack. High speed aircraft use this quality for reducing drag at high traveling speeds (Luckering, 2019).

Figure 3. Vortices forming above the wings of Concorde during landing and take-off.

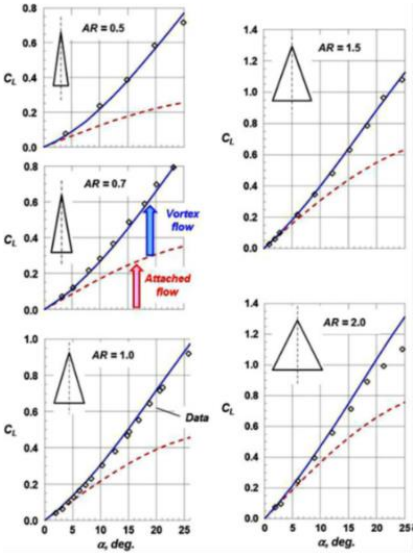

Vortex-lift predictions for delta wings. M = 0. [Polhamus, NASA, 1966]

Figure 4. Vortex-Lift effects for delta-wings (Polhamus,1966).

This low resistance value for small angles of attack could be beneficial for a sailing vessel design that aims at minimizing additional drag and operates at relatively small leeway angles.

3.1.2 Vortex-Lift Effects at a Traditional Sailing Yacht

In a first study in 2011 the principle of vortex-lift was analyzed for traditional long-keel yachts that show a steady keel-rake. The presence of a significant vortex system, that creates a low-pressure field within its core - similar to the observed vortex-systems of a delta-wing airplane - could be proven (Wagner, 2011).

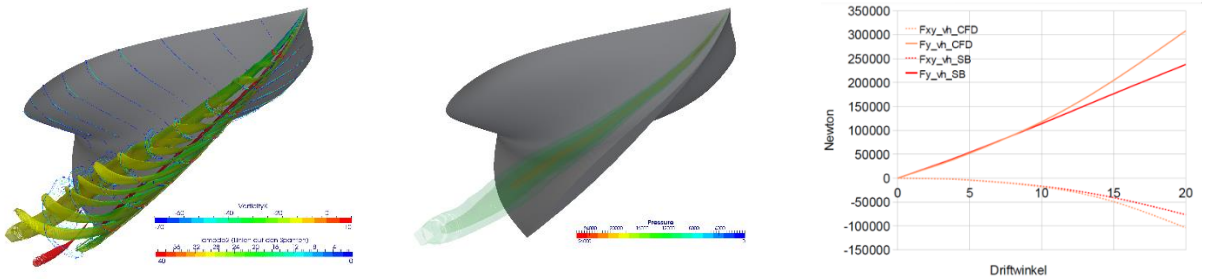

Figure 5. Vortex at yacht hull with keel rake (right), low-pressure at vortex core (middle), empiric-analytical and numeric calculated cross-force and drag (right).

This first study compared the CFD-RANSE calculated results for cross-force and drag at a raked long-keel yacht towards the empiric-analytical calculation procedure ‘slender-body-theory’ (SB). The calculation procedure uses sectional data from the hull (beam, draft and sectional area) to calculate cross-force, induced drag and yawing moment (Schenzle, 2010). The comparison showed that the analytical calculation procedure gives good results up to ten degrees of leeway angle. Above ten

degrees the calculated curves deviate. The effects of additional vortex-lift and drag could be observed within the CFD-RANSE based calculation results for cross-force and drag, and also within the vector-field visualizations (Fig. 5).

3.1.3 Transferring the Delta-Wing Concept Towards the Keels of a Modern Ship Hull

Based on these first findings for vortex-lift effects at the raked keels of traditional sailing vessels, a second research project was undertaken in 2014 to investigate possible design options of such a delta-wing keel system for large commercial cargo ships. The principal idea was to attach the low aspect-ratio delta-shaped keels at both sides of a modern flat bottom hull. The side-ward attachment can be realized without any increase of draft. Further, as soon as the vessel leans over to one side due to the cross-force from the wind propulsion system, this sideward positioned keel will effectively increase the draft of the vessel. The higher the heeling angle the higher will be the added draft and thus effectiveness of the keel system is likely to be increased. Its position in luv (from a hydrodynamic perspective) of the hull leads towards a clean and undisturbed inflow. Compared to a centred keel system where the water-flow is slowed down by the presence of the hull, this sideward position could be beneficial for performance of the system. The big question is if the second keel, positioned behind the hull, will remedy the advantages of the luv-ward positioned keel or if in total a positive benefit remains.

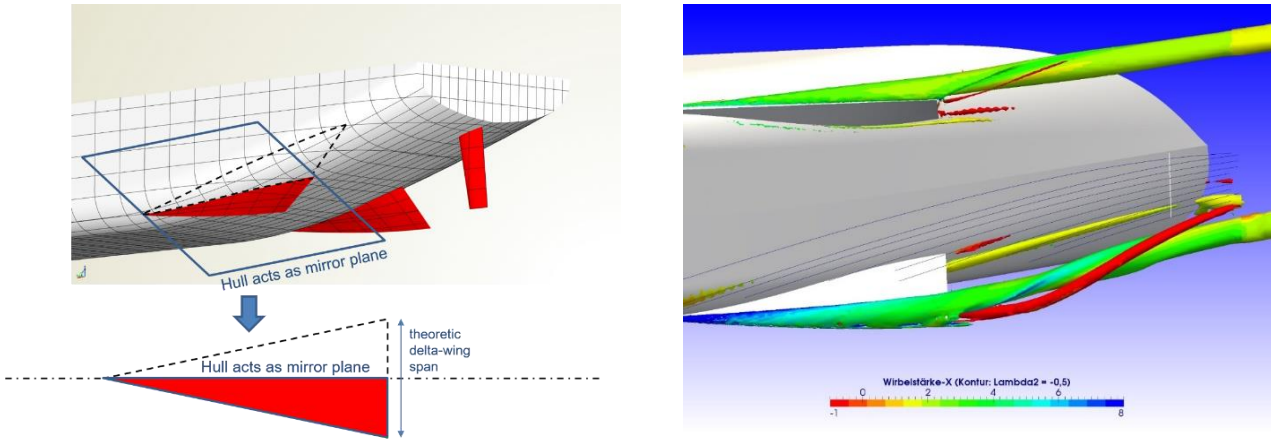

Figure 6. Design concept for delta-wing keels at a flat-bottom hull for a commercial cargo-ship.

The hull itself acts in that sideward attached configuration as a mirror plane. Only one half of the ‘theoretical delta-wing’ is attached to either side of the hull. The span of these sideward attached keels is limited by the shape of the hull. If attached in the vicinity of the mainframe, the bilge radius limits the maximum span of the keel. The further these keels are moved towards the aft, the higher can be the effective span of the resulting delta wing whereby aspect-ratio is increased. The total size of such designed keels can be significantly larger, while draft of the vessel is not increased at all. Further, the concept allows to specifically design the keels according to the requirements given by the wind propulsion system by choosing correct size and longitudinal position. The concept can be realized for most modern ship hull geometries. Even retrofits to existing hulls are thinkable, since these completely passive keels are attached solely to the outside of the hull. Inside of the ship no additional space is required.

3.2 Geometries

The basis for the numerical shape variation and investigation is a parametric design environment that allows to create similar shapes by changing single design parameters. For this study a parametric model was created within the design environment of CAESES from Friendship Systems. The base hull is varied by changing keel-rake from zero to two meters. This change affects of course the lines-plan of the hull, but main parameters are kept identical: length, beam, average draft, displacement, waterline and area, mainframe, deck and transom are identical for both versions. All appendage systems that are analyzed within this study are attached towards this base hull design.

In that way the effects of the appendage systems on vessel performance can be analyzed and compared, Focus lies on the effects caused by the appendage systems, rather than optimized base hull performance.

3.2.1 Basic Ship Hull Geometry

The basic hull that was used for all calculations is similar to the main dimensions of the 'Ecoliner Concept' (Dykstra Naval Architects, 2009). Table 1 shows the main parameters of the base hull.

Table 1. Main parameters for base hull

Length between perpendiculars	130.0	m
Beam	18.2	m
Average draft	6.5	m
Displacement	11000.0	t

Since keel-rake is traditionally used to move the $C_{E,hydro}$ for the hull further aft (Schenzle, 2010), the large majority of calculations are done for a hull including a keel-rake of two meters. Keel-rake further provides additional draft for the aft-ship, leading to increased draft for the appendage systems compared to the design variants on even keel.

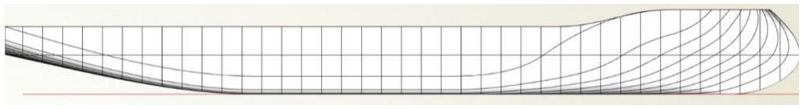

Figure 7. Bare hull, no keel-rake.

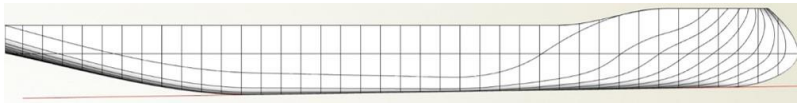

Figure 9. Bare hull, keel-rake of 2m.

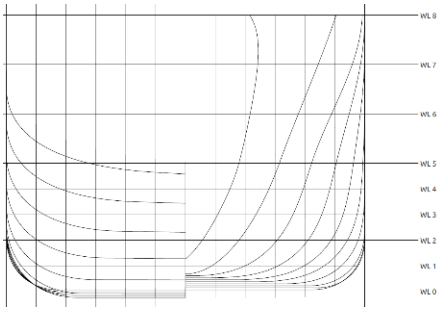

Figure 8. Sections for a keel-rake of two meters.

3.2.2 Three Different Keel Design Concepts

As a reference for comparison, two other keel concepts were analyzed within the study and compared towards the vortex-lift based design concept. The conventional approach is a center-skeg variant in combination with standard bilge-keels (CS-v1). A more specialized concept is the double fin positioned to both sides of the centered propeller and rudder as far out as possible, similar to the concept used by the E-Ship 1 from Enercon, but in this study these additional fins are considered as fixed structural parts, not rotatable like a rudder (DF-v4). The fins are aligned to the streamlines such that initial drag is minimized on a straight course without leeway angle. Focus lies on two delta shaped bilge-keel variants. The first is a relatively large appendage system that starts forward of the mainframe and extends far aft into the aft-ship region. This large keel system allows to create high cross-forces that are able to counter a major wind propulsion system (SK-v4). The second delta-shaped side-keel configuration (SK-v7) is a much more moderate version that is positioned far aft in the aft-ship region but still well forward of the propeller and rudder position (referred to as SK-v7). The two side-keel variants show exemplary the potential of such a keel system. Any size in between can be realized as well. Table 2 presents the geometric data for the appendage system variants.

Table 2. Appendage systems data table.

	Angle to vertical	Length	Surface area
Bilge keels for variant CS-v1 and DF-v4	45°	38.1 m	61.7 m²
Center-skeg for variant CS-v1	0°	39.0 m	231.8 m²
Double fin for variant DF-v4 (per fin)	20°	7.0 m	90.5 m²
Delta-shaped side-keel for SK-v4 (per keel)	45°	62.5 m	252.4 m²
Delta-shaped side-keel for SK-v7 (per keel)	45°	19.8 m	91.6 m²

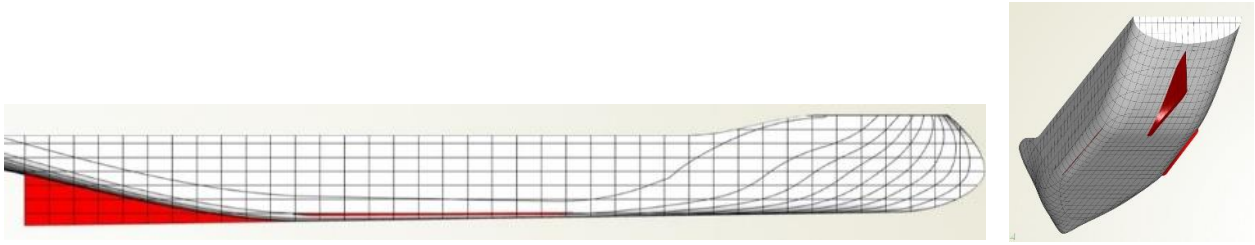

Figure 10. Center-skeg with bilge-keels (CS-v1).

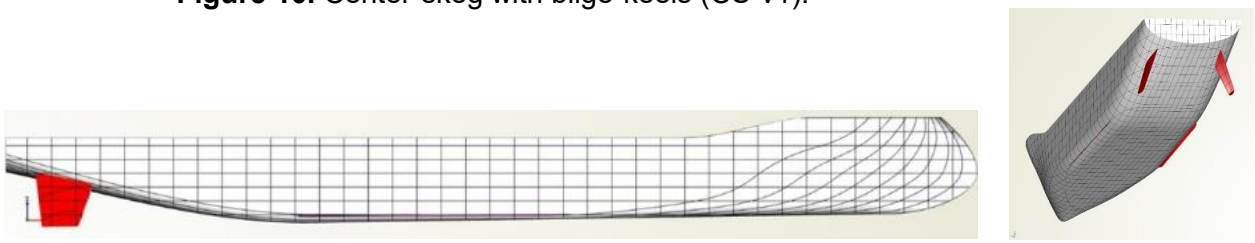

Figure 11. Double fin with bilge-keels (DF-v4).

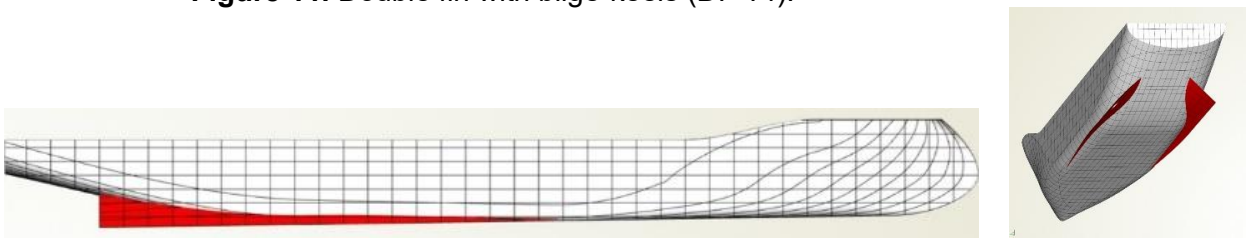

Figure 12. Large delta-shaped Wagner-Keels (SK-v4).

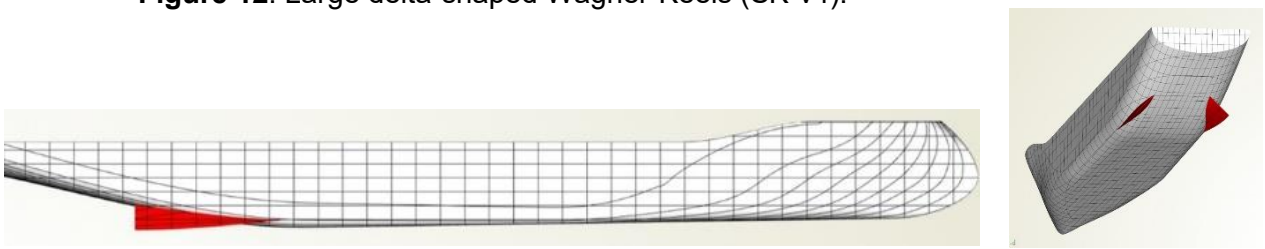

Figure 13. Small delta-shaped Wagner-Keels (SK-v7).

3.3 Calculation Environment

In order to evaluate and compare the different keel variants, the hull-polar-curves (C_L-C_D-curve) need to be created for each design variant and floating condition. The polar curves are obtained by variation of the leeway-angle in five steps from zero to fifteen degrees. Further, heeling angle and trim (design keel-rake) is varied for the most promising variants in order to analyse behaviour due to changing heeling angles and to evaluate the effects of trim or keel-rake on vessel performance. All calculations are based on the numerical concept of the Reynolds Averaged Navier Stokes Equations'(RANSE), that also allows detailed field analysis of the flow and pressure fields. Further insights are gained by analyzing the changes in the flow around the hull caused by the keel system and its effect on the distribution of forces compared to the bare hull.

3.3.1 CFD-RANSE Based Calculation Procedure

For all calculations within the basic research study a CFD-RANSE based calculation environment is applied. The algorithm used for these calculations is the FreSCo+ code, developed at the Institute for Fluid-Dynamics and Ship-Theory (FDS) at TUHH in Hamburg. FreSCo+ is a volume of fluid solver, based on RANSE .The solver is run on a numerical grid that defines the volume of fluid of the calculation domain. This domain is basically a large box with the ship at its center (Fig. 14).

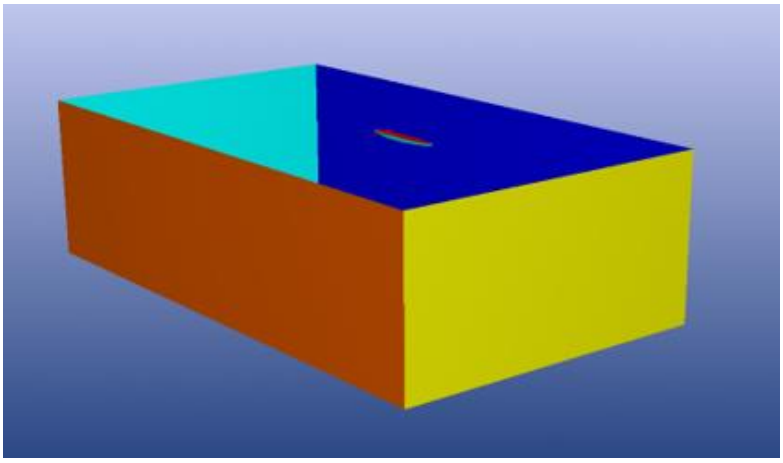

Figure 14. Calculation domain.

The volume between ship and the boundaries of the domain box is then discretized with the software HEXPRESS from NUMECA. Focus of this study lies on the details happening around the appendage systems and in comparing different design approaches and appendage layouts. To cover all these details a very fine discretization of the calculation domain is required, especially within the vicinity of the appendage systems, leading to a high number of cells of around 8-16 million cells for each variant.

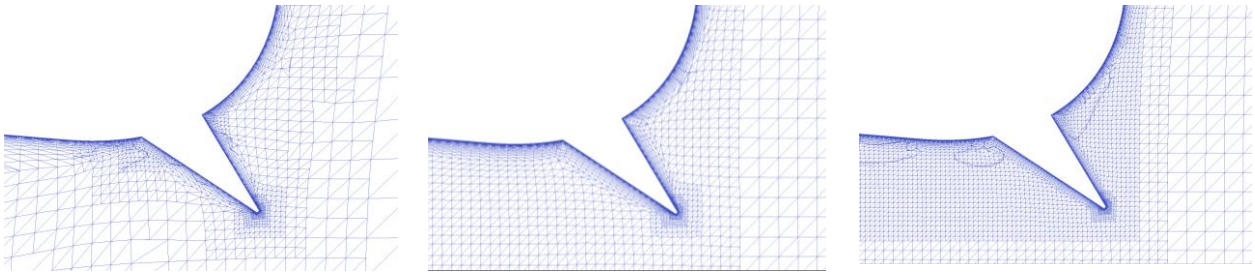

Figure 15. **grid refinement, mainly focused on expected vortex volume.**

A high number of cells is located in the hull surface boundary layer and within the turbulent flow regions of hull and appendage system. Fig. 16 shows the error of the calculated drag- and cross-forces for different grid refinement levels, given in percentage towards the finest grid.

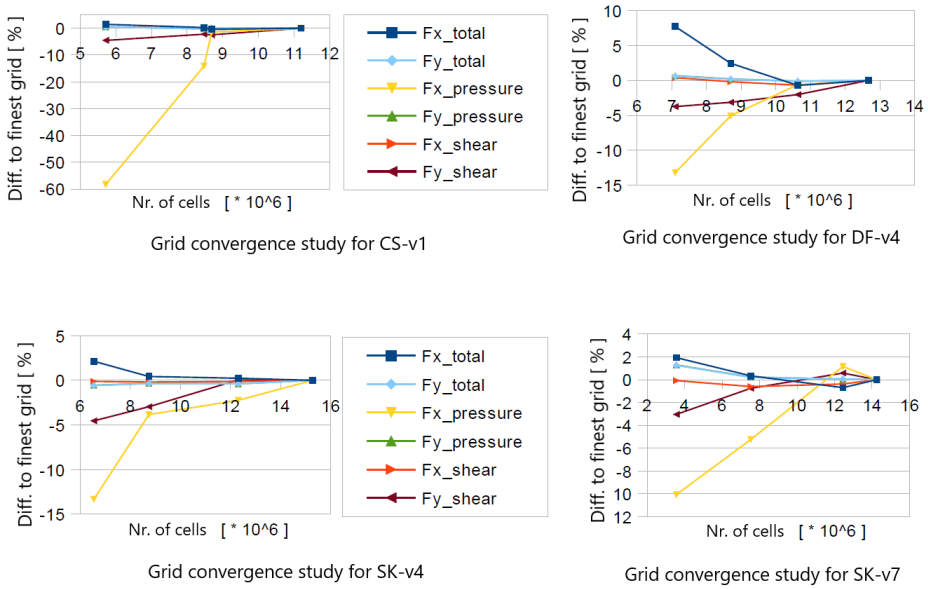

Figure 16. Grid convergence studies for the four appendage variations.

The quality of the boundary layer cells and the $Y+$ reached values at the first cells are displayed exemplary for variant SK-v4 in Fig. 17.

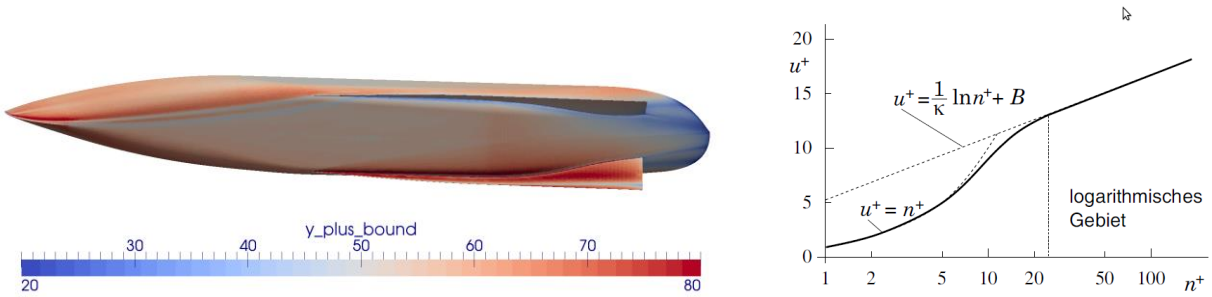

Figure 17. $Y+$ distribution, based on the logarithmic wall law.

For the variations of the leeway angles (creation of the polar curves) the calculation is repeated on the same grid but with changed inflow velocity vectors, whereby errors resulting from changing grids are avoided. Further, all calculations are done in full scale for this 130 m vessel, to avoid errors due to scaling effects, especially concerning turbulent flow in the vicinity of the boundary layers and the expected forming of vortices at the appendage systems. In total, more than 150 CFD-RANSE based calculations were performed for a large variety of grid, shape and inflow variations (Wagner, 2015).

3.3.2 Calculation Concepts for Efficient Appendage System Analysis

Even though the interference effects between appendages and the ship-wave system can be neglected due to relatively low Froude-numbers below 0.2 (Schenzle, 2010), the ship-wave system itself still has significant influence on the total forces and moments. In an additional calculation series for the hull without appendages, but including the free surface (two phase simulation series) the effects caused by the ship-wave system are calculated.

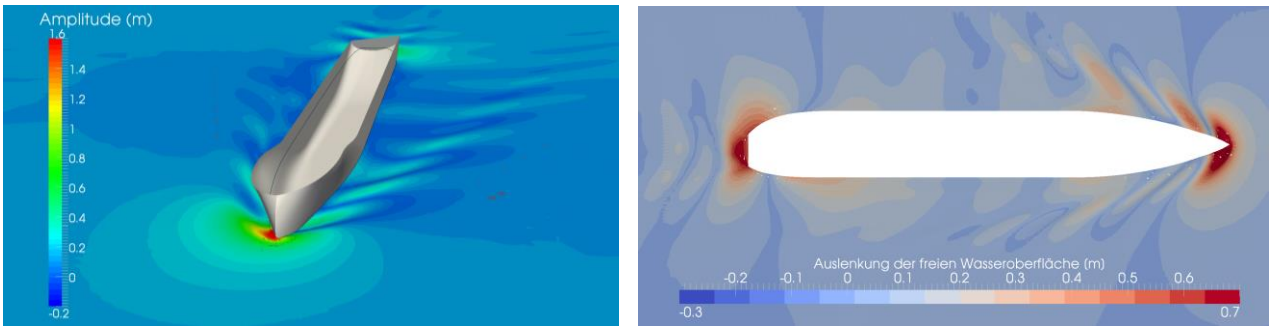

Figure 18: Calculation series for bare hull including free surface effects.

The result of the free surface calculation series is a cross-force drag polar curve for the bare hull including the effects of the ship-wave system. By subtracting the results (forces and moments) of the single-phase calculation (domain is cut at water-plane level) from the results obtained by the two-phase calculation series including the free surface effects, the sole effect of the ship wave system is isolated (referred to as R_w in the following diagrams, see Fig. 19). The resulting forces and moments for the ship-wave-system are then used to compliment the calculated results of all other single-phase calculations (Fig. 20). The separated calculation procedure is an efficient way to analyze the appendage systems in greater detail, while computing time is reduced significantly.

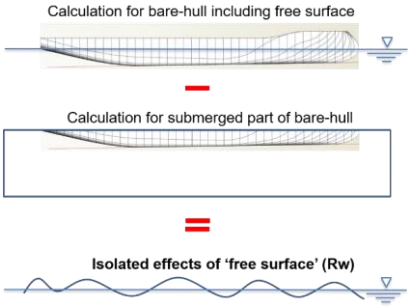

Figure 19. isolate effects caused by the ship-wave system

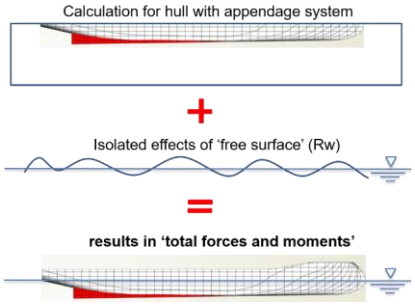

Figure 20. add the isolated effects from the ship-wave system to approximate total forces and moments

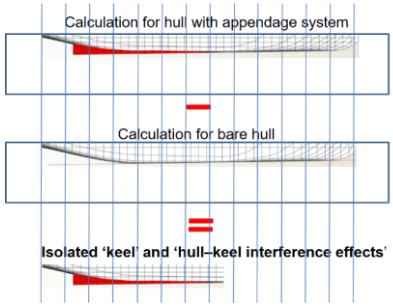

Figure 21. isolate effects caused by the appendage system

Due to flow interference effects between hull and any kind of appendages it is not possible to tell exactly what part of the results (forces and moments) is caused by the flow around the keels (appendages) and what is caused due to the changed flow around the hull triggered by the presence of the attached appendage system. However, some details can be obtained by analyzing the 'change' caused by the appendage system, compared to a calculation for the hull without any appendages. The resulting difference between the two calculations series results in the isolated effects that the keel system has on the performance of the hull (Fig. 21). This difference between the two calculations series includes therefore the effects of the 'keel itself' as well as the 'interference effects' caused by the attached keel on the flow conditions around the hull. Further insights into the generated forces are obtained by virtually cutting the ship longitudinally into sections. The concept allows to evaluate the distribution of the generated forces and moments.

3.4 Calculation Results – Compare Keel Design Concepts and Design Variants

Main results from the RANSE based calculations are the recorded forces and moments for the four different appendage configurations. Based on these calculated forces and moments a first comparison between the four analyzed design variants can be made. Fig. 22 shows the differences between DF-v4, SK-v4 and SK-v7 compared to the base variant CS-v1 (center-skeg with standard bilge-keels).

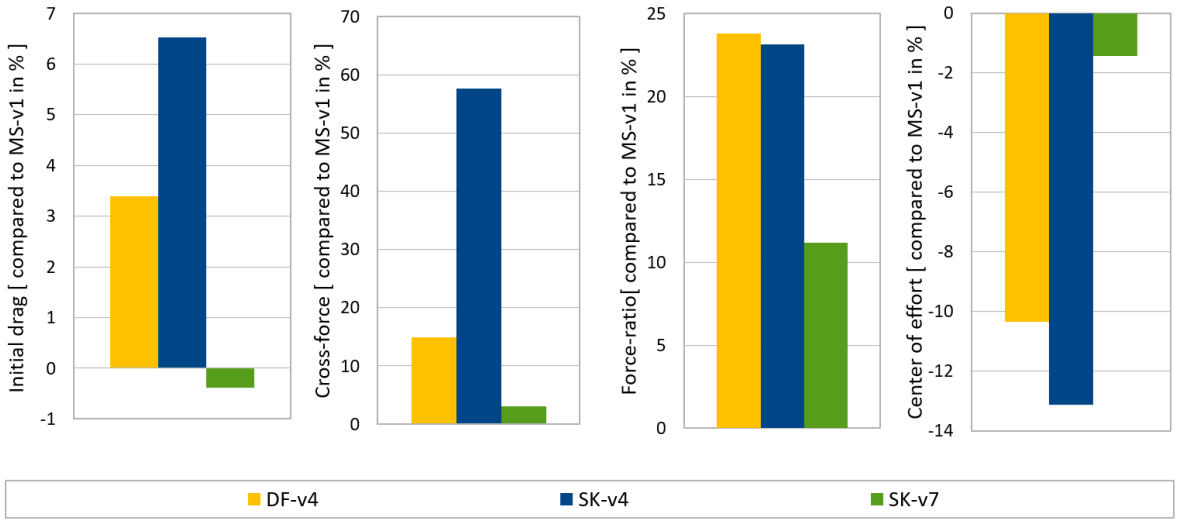

Figure 22. comparison of the key performance indicating parameters of the four selected design variants.

For this first comparison, initial drag was analyzed for a no heel and zero leeway angle condition. Cross-force, force-ratio and the hydrodynamic center of effort were measured at a heeling angle of 5° and a leeway angle of 10°. These two floating conditions have been applied as well for several other keel design variants [Wagner, 2015] and based on the results, the most promising candidates were selected for further investigations as presented in the following chapters. SK-v4 represents the best analyzed variant for high cross-force values and also high force-ratios and thus represents a very large system that is capable of handling large aerodynamic side-forces. SK-v7 at the other hand represents a much more moderate design solution that is especially interesting due to low initial drag values.

All three variants show higher cross-force values, force-ratios and also a more favorable position of the centre of effort that lies further aft than the center-skeg version (CS-v1) that serves as baseline and reference. Especially for SK-v4 and the double-fin variant (DF-v4) force-ratio and center of effort show significantly better values. The large side-keel variant shows much higher cross-force values, but that benefit comes along with a clearly increased initial drag value. Concerning initial drag it can be observed that this value is lowest for the small side keel variant (SK-v7) followed by the reference CS-v1.

Also, all these indicator figures are important for the sailing capabilities of the ship, it is difficult to decide which one will work best. The only safe information that can be concluded from this comparison is that SK-v7 will perform better than CS-v1 since its performance indicating values are better in all four categories, especially concerning the force-ratio. Concerning the other variants further information is required and will be provided and discussed in the following chapters.

3.4.1 Hydrodynamic Lift and Drag Polar Curves

Hydrodynamic lift and drag curves for each series are an excellent basis for comparing the efficiency of the different appendage systems. Together with the separately obtained resistance curve for the hull and suitable concepts for sea-state resistance calculation, these curves can be used for efficient vessel performance predictions. The curves give the initial resistance, induced resistance and cross-force for varying leeway-angles. Initial resistance is the resistance of the hull without any leeway angle (smooth water towing resistance at design speed). As soon as the vessel is heeled to one side, the symmetry is lost, and additional force components are created. A cross-force that is oriented perpendicular towards the direction of the flow and additionally the induced drag, adding to the initial resistance in direction of the flow. The hydrodynamic lift and drag curves are calculated for a steady heeling angle of five degrees and for leeway angles of up to 15°.

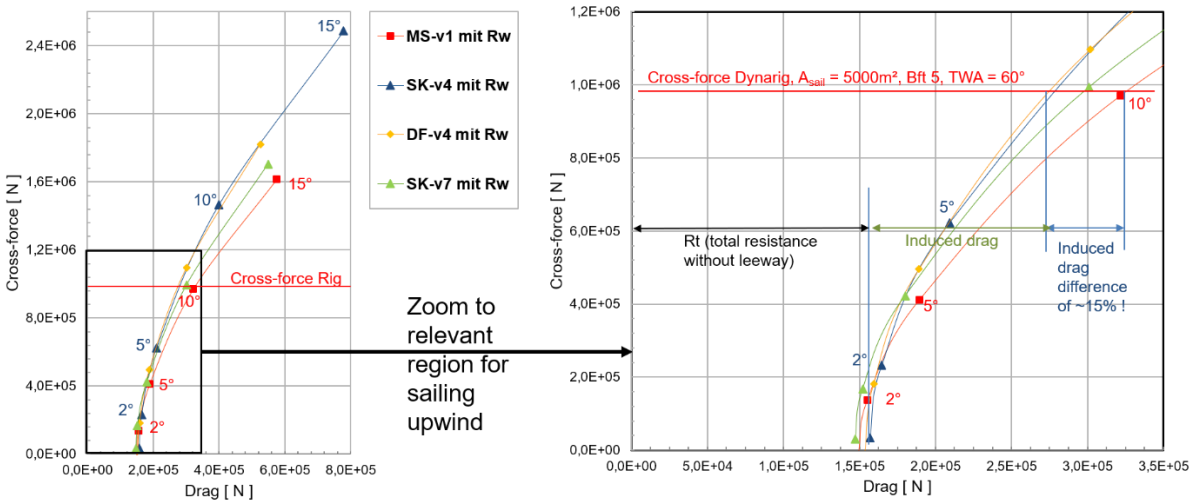

Figure 23. Cross-force-drag curves: comparing variants, large cross-forces.

In order to classify the results, an approximated cross-force from a large Dynarig wind propulsion system (WPS) is drawn into the diagrams (Fig. 23 and Fig. 24). This cross-force from the WPS needs to be countered by the hydrodynamic layout of the vessel in order to reach the equilibrium of forces and moments, whereby differences for the center of efforts need to be equalized by the rudder. The total drag difference of variant SK-v4 and variant DF-v4 compared to variant CS-v1 is about 15%, leading effectively to faster sailing speeds. SK-v7 lies somewhere between with an additional induced drag value of about 7%. Due to the larger keel areas of SK-v4 the leeway angle (markers on the displayed curve for each series are 0°, 2°, 5° 10° and 15°), required to reach the cross-force demanded by the WPS, is significantly lower. If overall performance of the different variants is to be evaluated, then cross-force and induced drag alone are not sufficient since the initial drag values play an important part as well.

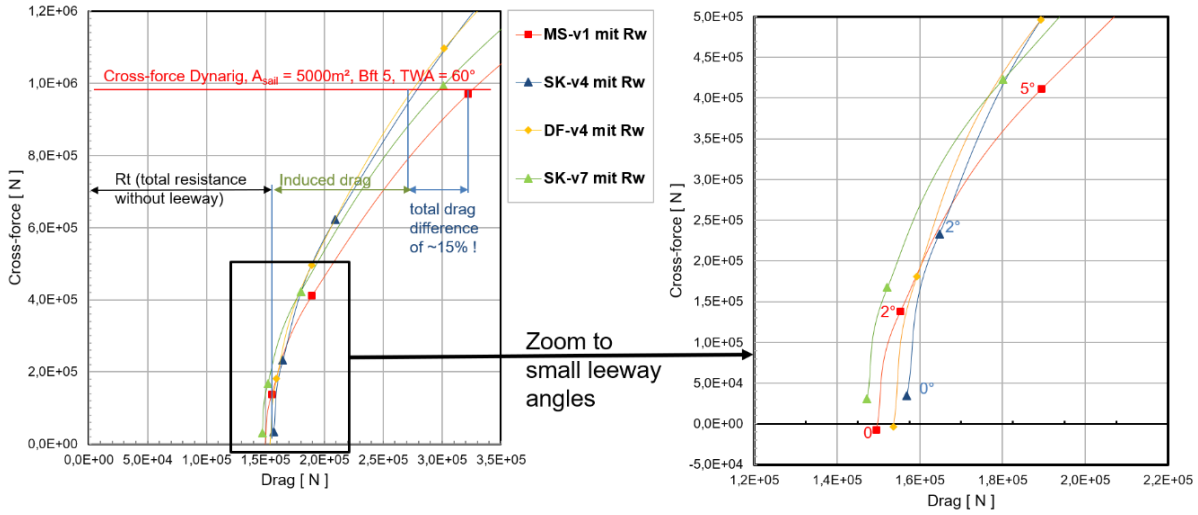

Figure 24. Cross-force-drag curves - compare variants and initial drag values.

Initial drag (compare 0° values in Fig. 24) of the two variants SK-v4 and DF-v4 is larger than for the center-skeg variant (CS-v1) and the small side-keel variant (SK-v7). Initial drag is important for sailing downwind or in engine mode where no cross-force from the WPS needs to be countered. SK-v7 shows the lowest initial drag values even though its surface area (data is shown in Table 2) is similar to the double fin variant (DF-v4).

SK-v7 gives the best results concerning total drag up to a cross-force level of about 4.0E+5 N. Above that value DF-v4 and SK-v4 perform better as outlined above.

3.4.2 Hydrodynamic Center of Effort

For further discussion of the results the $C_{E.hydro}$ needs to be considered as well. Due to the rather small layout of the rudder, compared to the large areas of hull and keel, the yawing moment equalizing ability is limited. If the required rudder angle is too large, then the reserve for manoeuvring the ship is compromised.

In general, it can be observed that the $C_{E.hydro}$ moves backwards for increasing leeway angles. Especially pronounced is this behaviour for CS-v1. For small leeway angles the $C_{E.hydro}$ lies at a far forward position of about 92% of L_{PP} for CS-v1. Variants SK-v4 and DF-v4 are already close to the estimated $C_{E,aero}$ at the required cross-force level. For SK-v7 and CS-v1 the rudder needs to move the $C_{E,hydro}$ backwards by around 10% of LPP in order to equalize the yawing moment of the WPS. Due to its ability to rotate, the rudder itself will have higher force-ratio values than hull and keel together. If cross-force and drag from the rudder is considered, then the total efficiency of the hydrodynamic layout will be increased, as long as the rudder is not overloaded. The same is true for a double or triple rudder configuration (E-ship One).

If the moderate side-keel variant (SK-v7) can provide the required cross-forces and $C_{E.hydro}$ together with a centred rudder at moderate rudder angles, then the economic benefit compared to multiple rudder design could make the difference for a commercially attractive system.

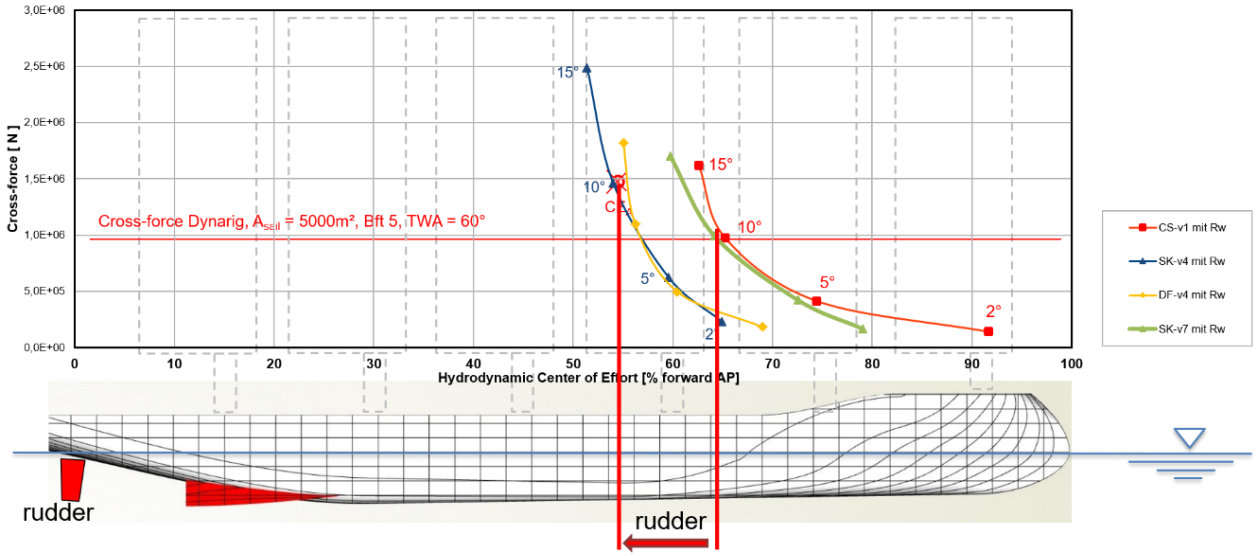

Figure 25. SK-v7 - position hydrodynamic center of effort, requirements for the rudder.

3.4.3 Visualization of Vector Fields

The RANSE based numerical calculation method allows detailed insights into the flow conditions around the hull- appendage systems. For a better understanding of what is happening at the appendage systems these vector-fields are analyzed in the following. The lambda-2 criteria is calculated and used to visualize vortices created at hull and appendage systems. The lambda-2 contour plot is colored with the vorticity rate in x-direction. The vorticity colors 'yellow to blue' can be seen on the main vortices, while orange/red is indicating secondary vortices rotating the opposite direction (negative vorticity values). The pressure plots show the effects of the vortices on the hull surface. Visible at the sides of the appendages is the low-pressure trace as a result of the low-pressure cores within these vortices

Center-Skeg Variant-1 (CS-v1)

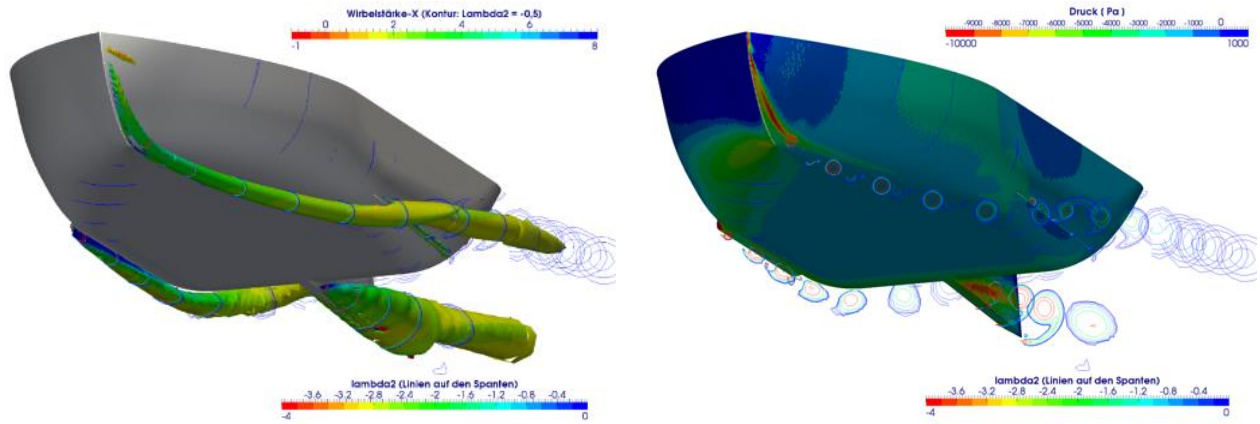

Figure 26. CS-v1 - Visualization of vortex systems (left) and pressure on hull-appendage surface (right).

Interesting are the observable differences between the luv-side (upstream) vortex and the leeside (downstream) vortex of the two bilge-keels. While the active luv-side vortex is attached to the keel, the lee-side vortex is created by the tip of the keel but almost immediately separates again. The large vortex at the center-skeg stays attached to the skeg and leaves a clearly visible low-pressure field at the side of the skeg.

Double-Fin Variant 4 (DF-v4)

The double fin variant (DF-v4), of course works completely differently in comparison. While the vortices at bow and bilge-keels look almost identically to the center-skeg version above, the fins function like a normal profile with suction and pressure side.

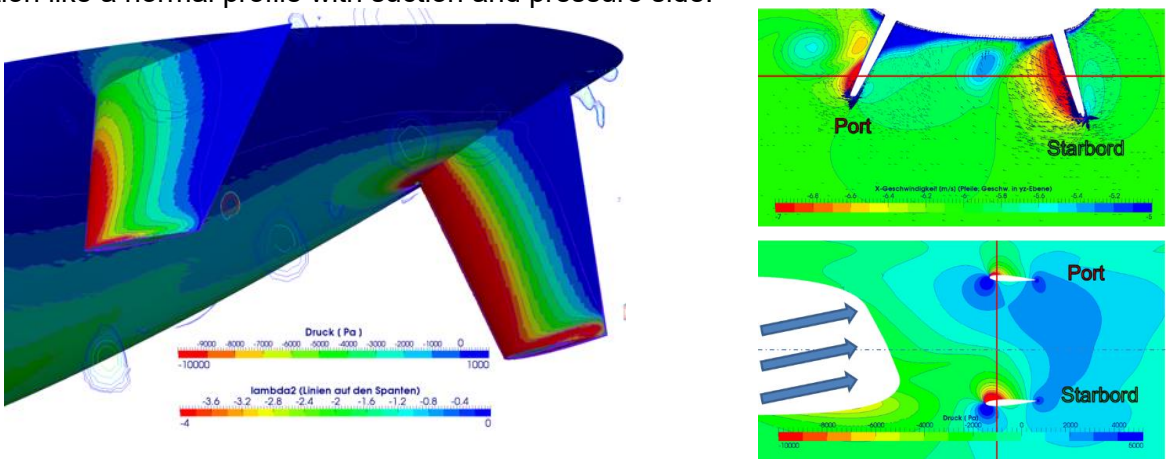

Figure 27. DF-v4 - Visualization of pressure on fin surface (left), velocity and pressure slice through fins (right).

The luv-side fin (starboard) creates high forces, due to the clean inflow conditions. The lee-side fin (port), however, is clearly compromised due to the presence of the hull upstream.

Side-Keel Variant 4 (SK-v4)

A major vortex is created at the active luv-ward side of the delta-shaped side-keel variant (SK-v4). This large vortex creates a low-pressure field at its core and leaves a low-pressure trace at the side of the keel.

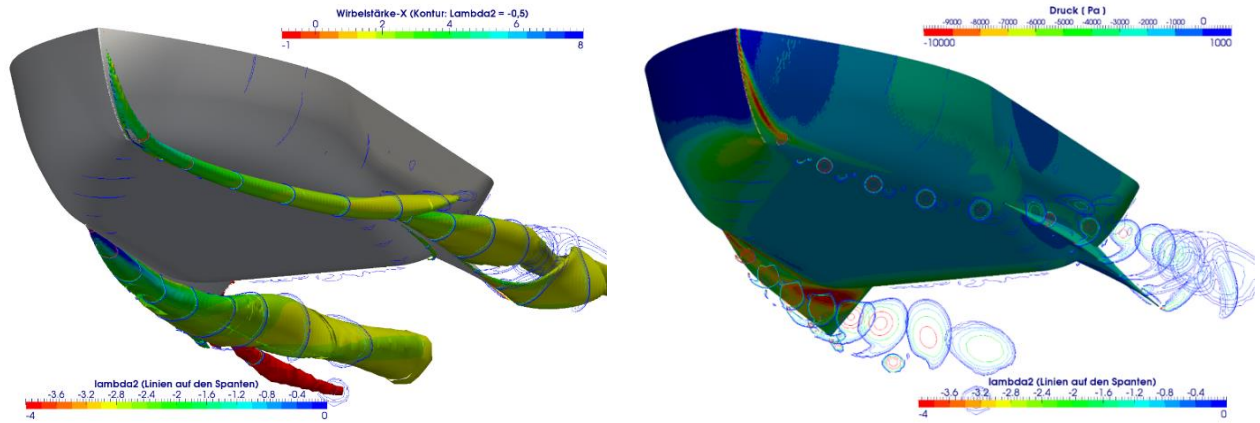

Figure 28. SK-v4 - Visualization of vortex systems (left) and pressure on hull-appendage surface (right).

Similar to the above-described keels, the bilge-keels the second keel behind the hull (downstream) also creates a large vortex, but this vortex separates from the hull and trails off with only minor effects on the pressure field of the hull.

The difference between the two vortices is made visible by slices through the calculated pressure and velocity fields (Fig. 29). The slice series shows the development of the upstream vortex (right hand side in the picture series), attached to the side of the keel with an increasing low-pressure field in its center. Also, interesting and in line with the theory of vortex systems observed for delta wing airplanes (Polhamus, 1966), is the accelerated flow within the core of this vortex. The leeward vortex (left-hand side in the pictures) behind the hull, shows just a minor low-pressure field at the center of the vortex. Velocity in x-direction within the vortex-core of the leeward positioned keel is slowed down.

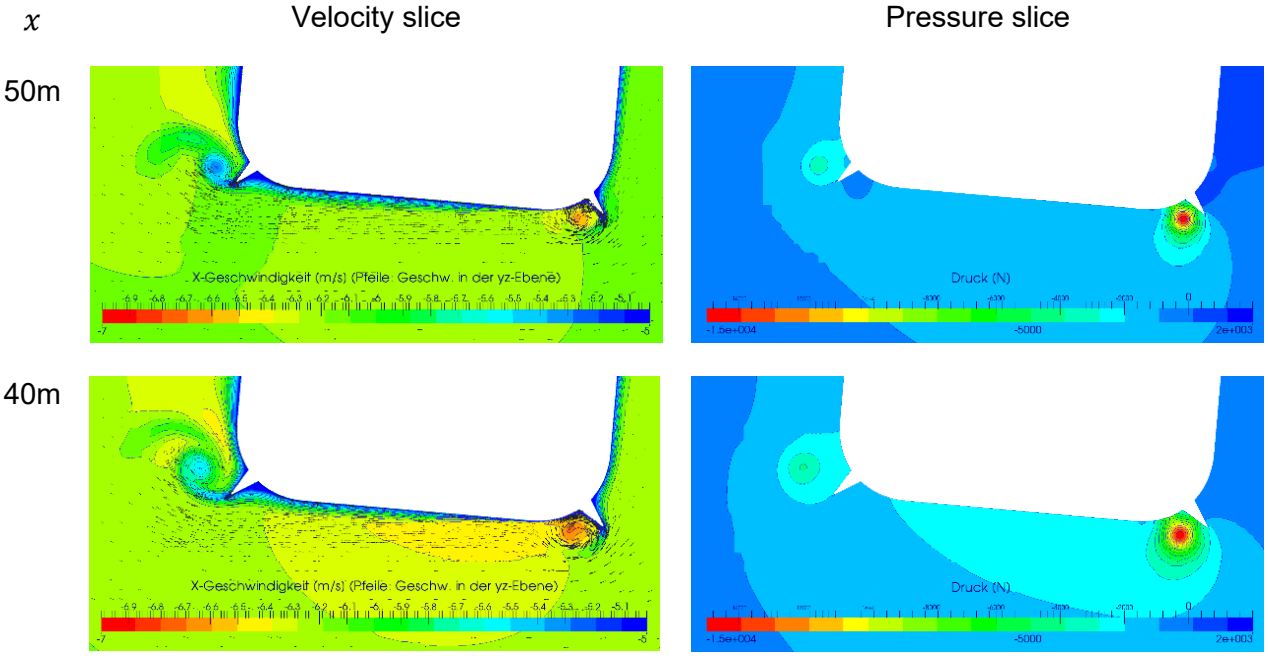

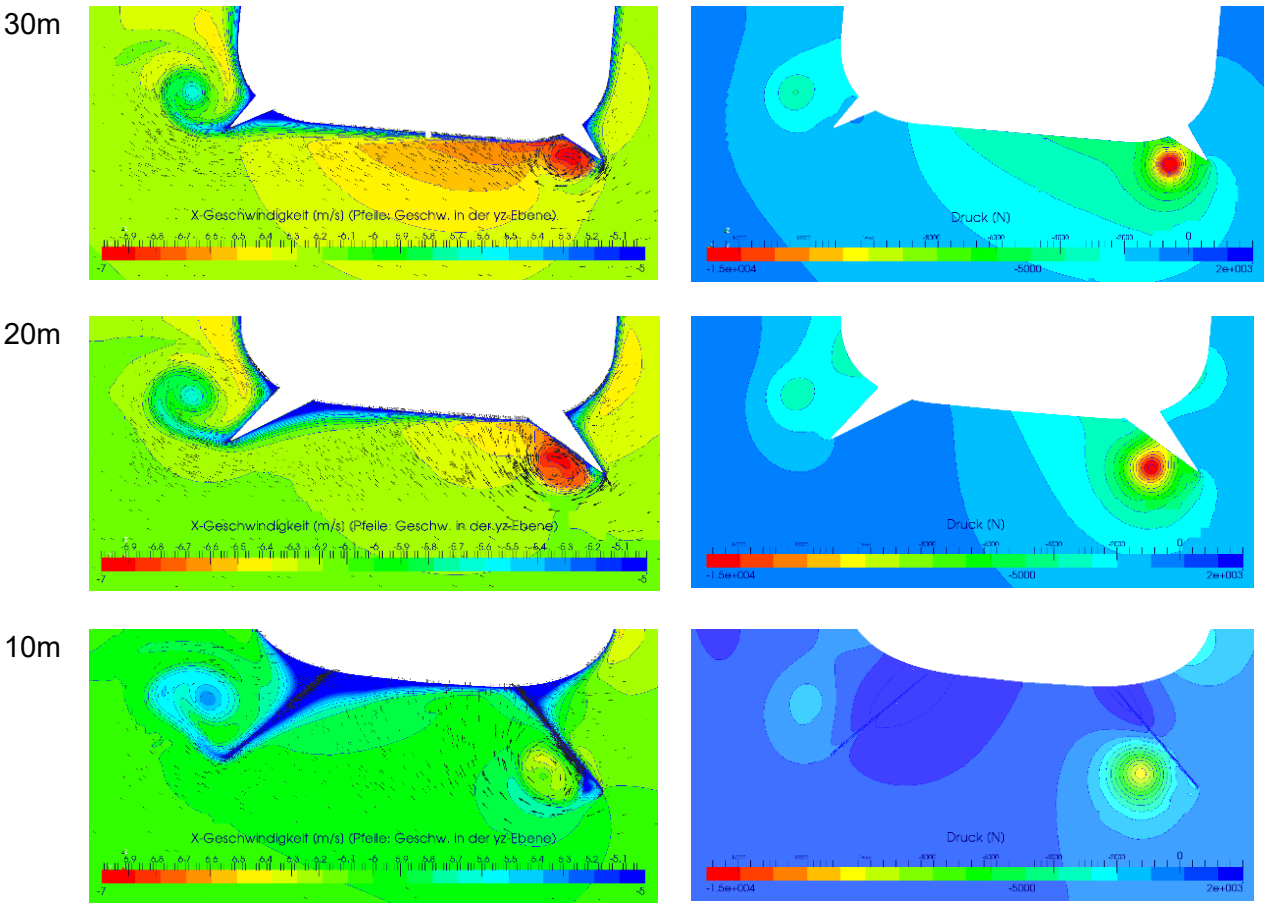

Figure 29. SK-v4 - slice series through velocity and pressure fields at different x-positions.

Side-Keel Variant 7 (SK-v7)

SK-v7 is designed with much shorter keels (length of only about 20 m). Main difference is the three times higher aspect-ratio compared to SK-v4 (compare Table 2), described above.

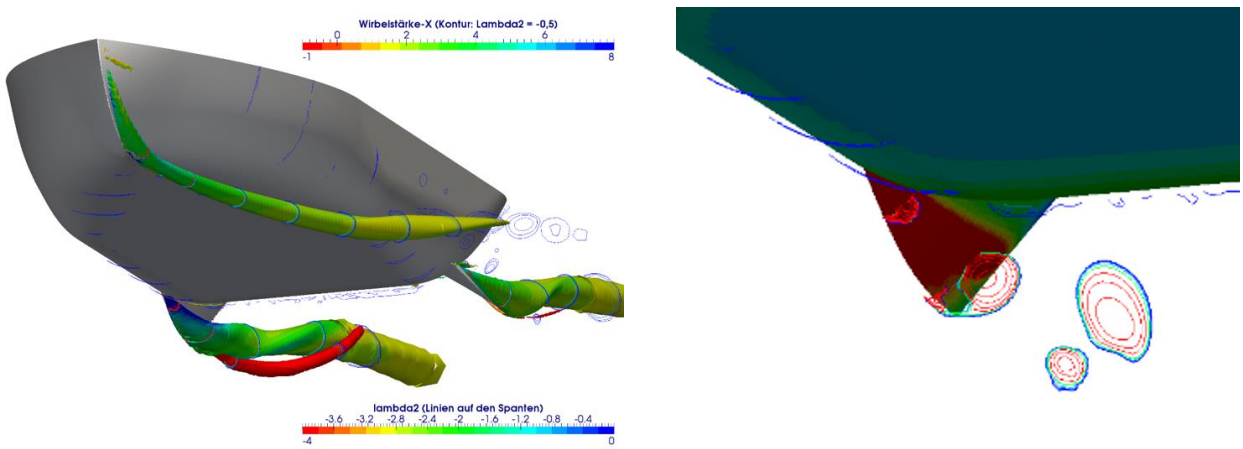

Figure 30. SK-v7 - Visualization of vortex systems (left) and low-pressure trace on hull-keel surface (right).

The low-pressure trace left behind at the surface of the keel (Fig. 30) is much more pronounced and covers large parts of the keel. The higher aspect ratio and the more delta-shaped contour of the keel clearly leads towards a faster developing vortex with an even more pronounced low-pressure core at its center.

3.4.4 Analyze Force Distributions from Bow to Stern

In the following the calculated forces and moments are evaluated section-wise by virtually cutting the ship into sections of one-meter length. This can be achieved by using a numerical filter for the longitudinal positions of each cell within the calculation domain. Such created force distribution curves show in more detail what is happening alongside the hull due to the presence of the different appendage systems. All following curves concerning the force distributions show the data for the submerged part of the hull only. Heeling angle is five degrees. Effects caused by the ship-wave system are not included. The section-wise calculated cross-force for the bare-hull (RoA) for different leeway angles is displayed in Fig. 31.

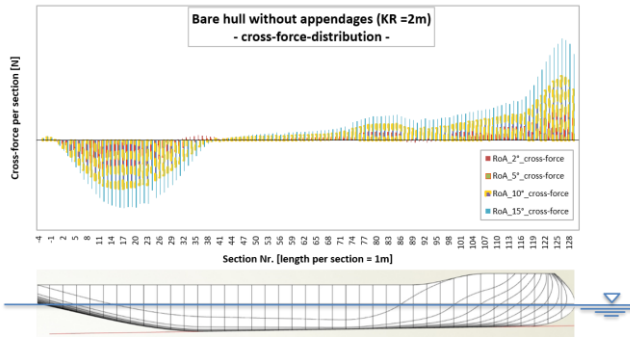

Figure 31. bare-hull - cross-force distribution (bar-chart).

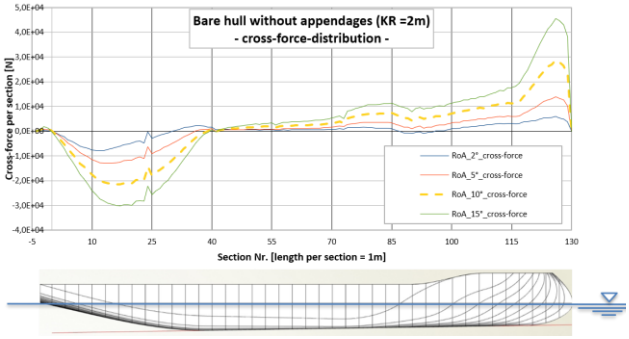

Figure 32. bare-hull - cross-force distribution (curve diagram).

In order to increase readability, the force-distribution data is displayed in the following as a lines diagram. The colors indicate the different leeway angles of 2° (blue), 5° (red), 10° (yellow, dashed) and 15° (green) The cross-force distribution for the bare hull (Fig. 32) shows a significant peak directly behind the bow of the vessel. In this region a large part of the total cross-force is generated. Due to the keel-rake of two meters, additional positive cross-force is generated further downstream as well. Behind the section of deepest draft at ~40m, the generated cross-force from the hull becomes negative (due to the absence of center-skeg and rudder). The negative force created behind section 40 thus counteracts the cross-force provided at the bow. The calculated $C_{E,hydro}$ for such a bare-hull design without any skeg or rudder will be far forward of the bow.

For the four different appendage systems (CS-v1, DF-v4, SK-v4 and SK-v7) the cross-force distribution curves are displayed in the same way (Fig. 33, Fig. 35, Fig. 37 and Fig. 39). If compared with the force-distribution curves calculated for the bare hull (Fig. 34, Fig. 36, Fig. 38 and Fig. 40), it becomes clear that the negative cross-force field in the aft-ship region is reduced and partly turned into positive cross-force due to the appendage systems.

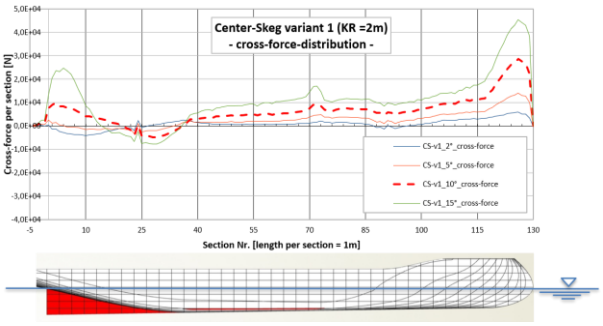

Figure 33. CS-v1 - cross-force distribution.

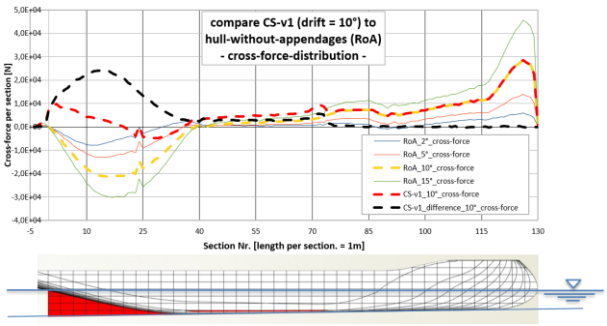

Figure 34. CS-v1 - cross-force distribution, compared to hull without appendages (RoA).

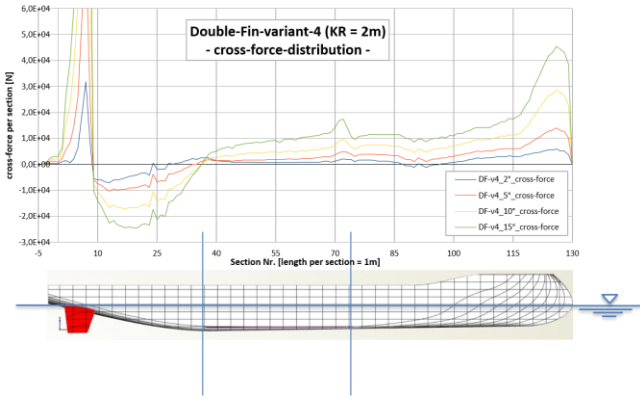

Figure 35. DF-v4 - cross-force distribution.

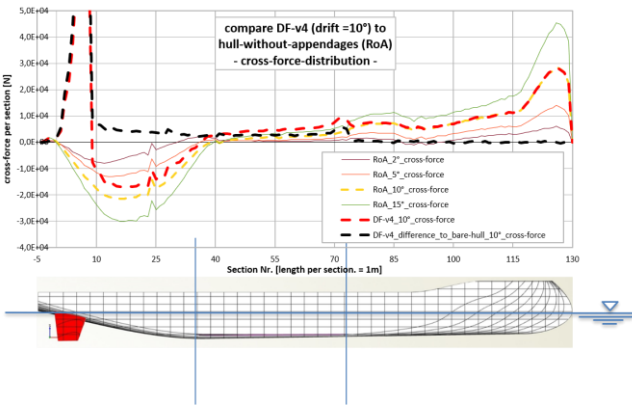

Figure 36. DF v4 - cross-force distribution, compared to hull without appendages (RoA).

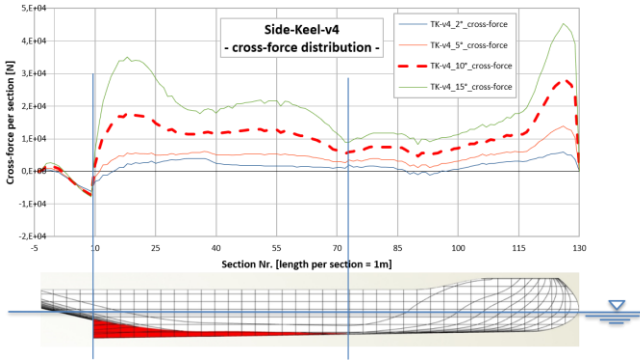

Figure 37. SK-v4 - cross-force distribution.

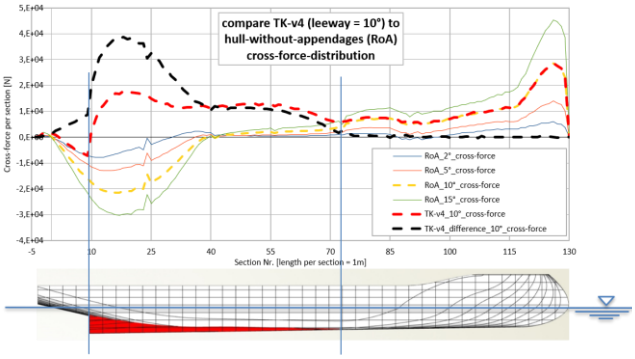

Figure 38. SK-v4 - cross-force distribution, compared to hull without appendages (RoA).

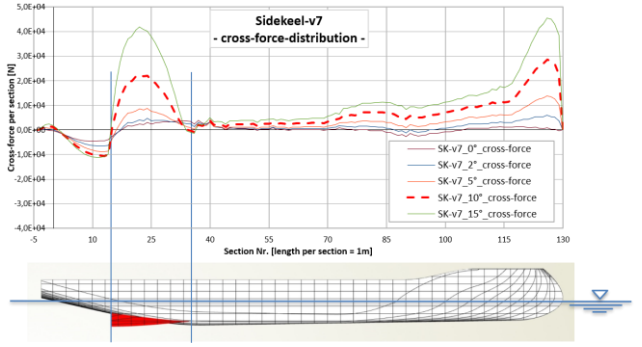

Figure 39. SK-v7, cross-force distribution.

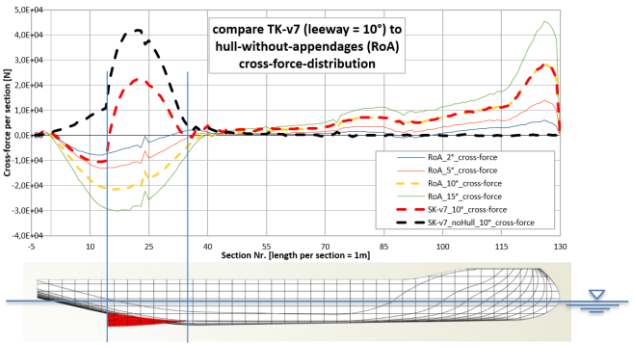

Figure 40. SK-v7 - cross-force distribution, compared to hull without appendages (RoA).

Forward of the appendage systems the cross-force distribution curves are identical to the curves for the bare hull for all four appendage systems. Behind the appendage systems however, the curves follow a cross-force distribution for a lower angle (compare red dashed 10° curve with the yellow 10° curve for the bare hull). The calculated difference towards the bare hull is given with the black dashed curves.

For the center-skeg variant (CS-v1) the inflow angle is reduced by the presence of bilge-keels and center-skeg by about 50% (compare the red dashed 10° curve towards the set of curves created by the bare hull in Fig. 34). The difference between the bare hull and CS-v1 is visualized by the black dashed curve. This difference thus represents the effect caused by the appendage system.

For the double fin variant (DF-v4) major parts of the generated cross-force are created at the two profiled fins (Naca-0412) behind section 10. The two bilge-keels behave identically to the bilge-keels displayed also for the center-skeg variant. Interestingly to observe is the fact that the effect of the

bilge-keels continues even behind the trailing edge of the bilge-keels. The presence of the bilge-keels thus reduces the inflow angle by about 20% for that specific design (DF-v4, Fig. 36). Thus, the bilge-keels have an additional positive influence by reducing the negative contribution of the cross-force created by the hull behind section 40. This effect is in the following called the 'hull-appendage interference effect'. Since the two large fins are positioned as far aft as possible, the positive interference effect on the hull is limited to the region of the fins themselves (behind section 10).

For the large side-keel variant 4 (SK-v4), the calculated cross-force difference (black dashed curve in Fig. 38) is gradually increasing with its highest value at section 17 (7 m forward of the trailing edge). The angle of attack for the region behind the keels is reduced by 80% due to the presence of the large keel system (compare curves for RoA_10°, RoA_2° and SK-v4_10°). A similar picture can be seen for the smaller side-keel variant SK-v7. The cross-force peak reaches a similar level a few meters forward of the trailing edge. Behind the keels a positive interference effect remains with flow-angle reductions of about 70%.

This major interference effect is displayed in Fig. 41 and Fig. 42. The red area represents the approximate part created by the keel system. The yellow part represents the hull-keel interference effects.

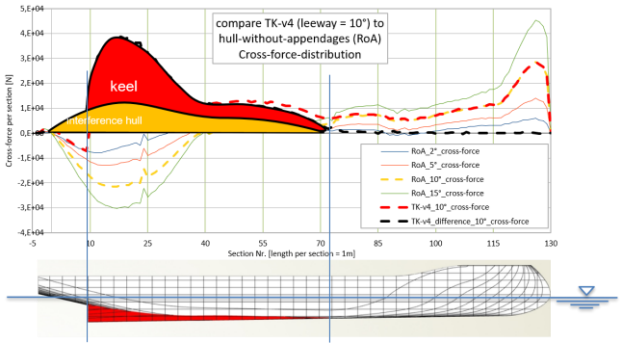

Figure 41. SK-v4 - cross-force distribution, hull-keel interference effects

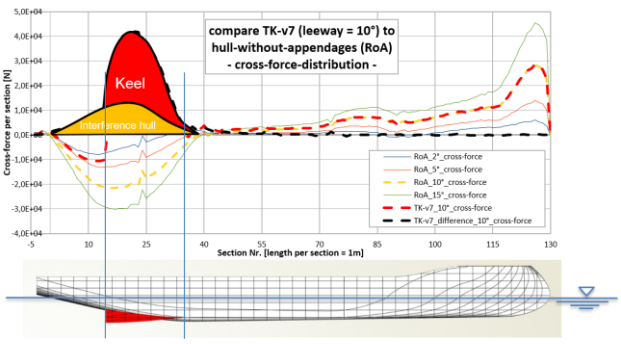

Figure 42. SK-v7 - cross-force distribution, hull-keel interference effects

It looks like the efficiency of this special keel system results in large parts also on the reduction of the negative cross-forces in the aft-ship region created by the hull itself. The same concept for calculating differences towards the bare hull is also applied to the drag-force distributions.

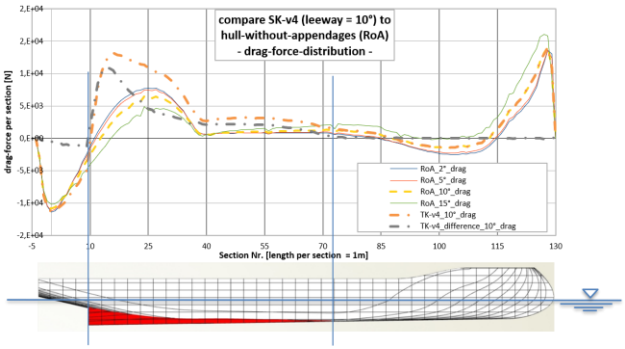

Figure 43. SK-v4 - drag-force distribution, compare to hull without appendages (RoA)

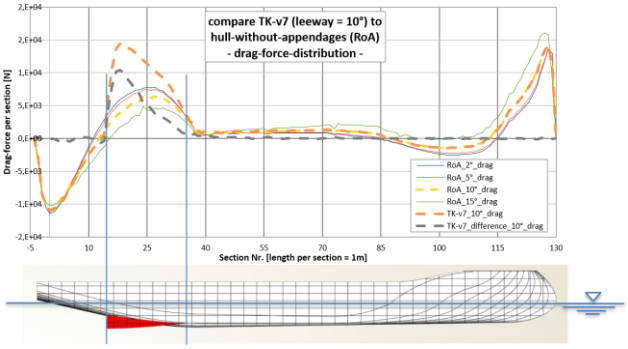

Figure 44. SK-v7 - drag-force distribution, compare to hull without appendages (RoA)

For the drag-force distribution (Fig. 43 and Fig. 44) the picture is similar than for the cross-force distribution. Forward of the keels, no difference is calculated. In the vicinity of the keels drag-force is increasing similar to the increase in cross-force. Interestingly is that the difference in drag-force behind the keel-system (dashed grey curve) is close to zero. No additional drag is created behind the delta-shaped appendage systems.

To complete the picture, the isolated appendage and hull-appendage interference effects are displayed in Fig. 45 as cross-force-drag coefficient curves. The dimensionless coefficients are calculated based on water density, vessel speed and the total appendage surface-area. For variant CS-v1 and DF-v4 this means that the bilge-keels are included as well.

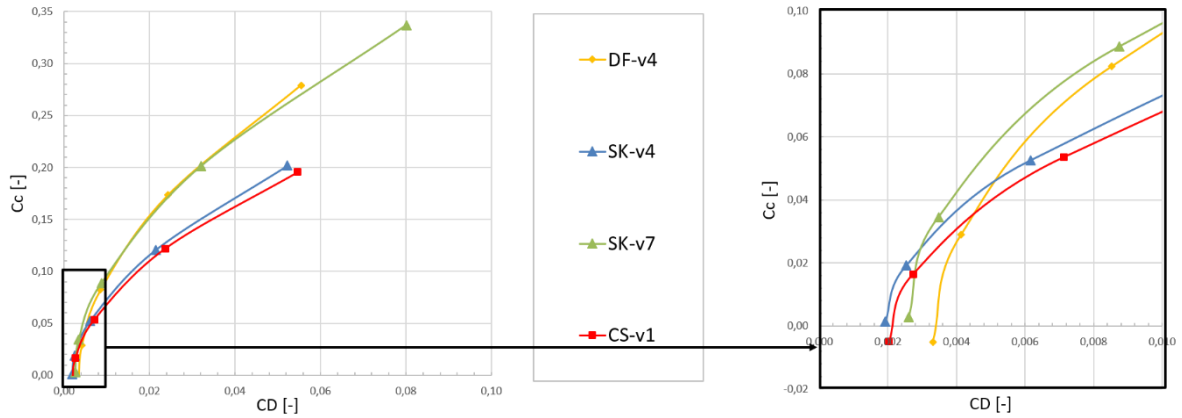

Figure 45. compare cross-force-drag coefficient curve for 'appendage' plus hull-appendage interference effects'.

Compared to the presented cross-force-drag curves for the complete ship (Fig. 23) the dimensionless cross-force-drag coefficient curves for the ‘appendage’ plus ‘hull-appendage interference effects’, clearly show the potential of the delta-shaped side-keel concept. Especially SK-v7 shows comparatively high-performance values. It is interesting to observe that despite the overall high performance of variant DF-v4, the initial drag coefficient for this appendage design variant is actually significantly higher than for the other three appendage systems. The reason for the lower initial resistance coefficients could be the almost horizontal leading edge of the delta shaped keel designs compared to the vertical leading edge of the double-fin design variant.

3.4.5 Behavior due to Keel-Rake Variation

All above discussed calculation series and appendage variations are calculated for a keel-rake of 2 m. In this section, additional series for even keels (KF of 0 m) are analyzed and compared to the above displayed data for the raked keels (KF of 2 m).

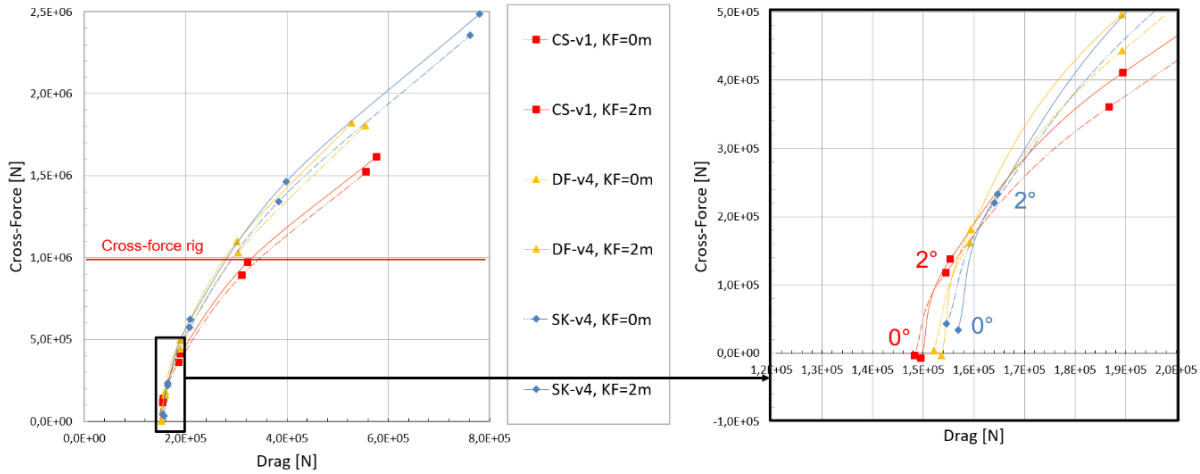

Figure 46. Effect of keel-rake on cross-force-drag curves.

As anticipated, keel-rake has a significant influence on performance of the ship. The cross-force drag curves are improved, indicated by a total drag reduction for leeway angles above two degrees and higher cross-force values resulting in increased cross-force-drag ratios. Initial drag at a leeway-angle of zero degree is increased only slightly for the raked keel variants.

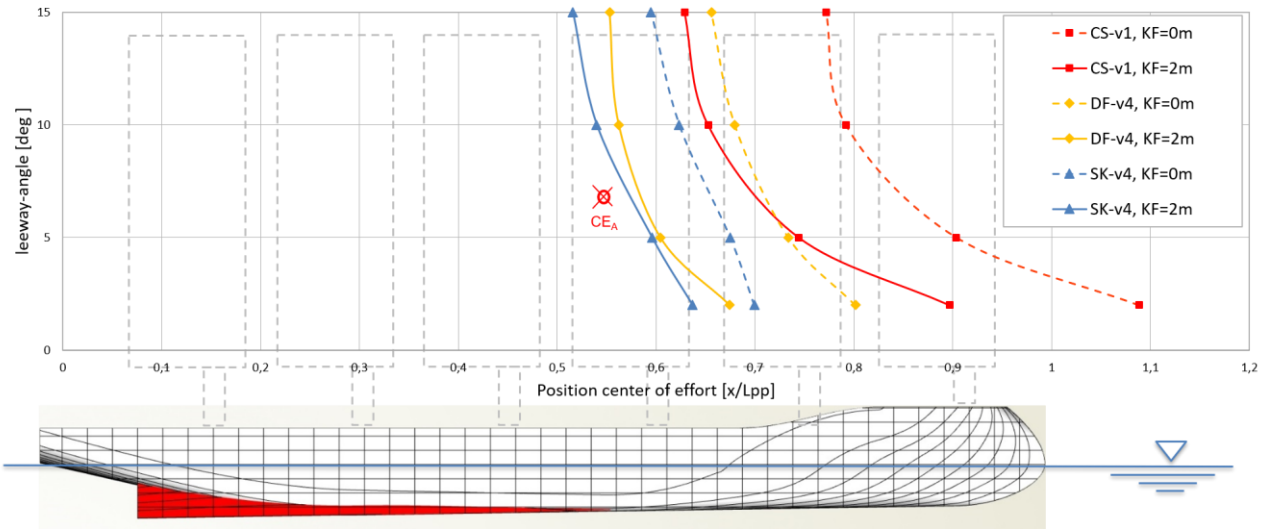

Figure 47. Effect of keel-rake on the hydrodynamic center of effort.

A major difference can be observed for the calculated position of the $C_{E,hydro}$. For all design variants the CE_H is positioned further aft by 7% to 18% if a keel-rake of two meters is applied. Partly this effect is caused by the hull itself. Additionally, the appendage systems can be designed slightly deeper, since draft at the Aft Perpendicular (AP) is increased due to the keel-rake design. The biggest difference is observed for CS-v1. The lowest influence is calculated for the large delta-shaped side-keel configuration (SK-v4).

3.4.6 Behavior due to Heel-Angle Variations

The influence of changing heeling angles has different effects on vessel performance for the different appendage design concepts. Fig. 48 displays the effect for an angle variation from 2.5° to 7.5°.

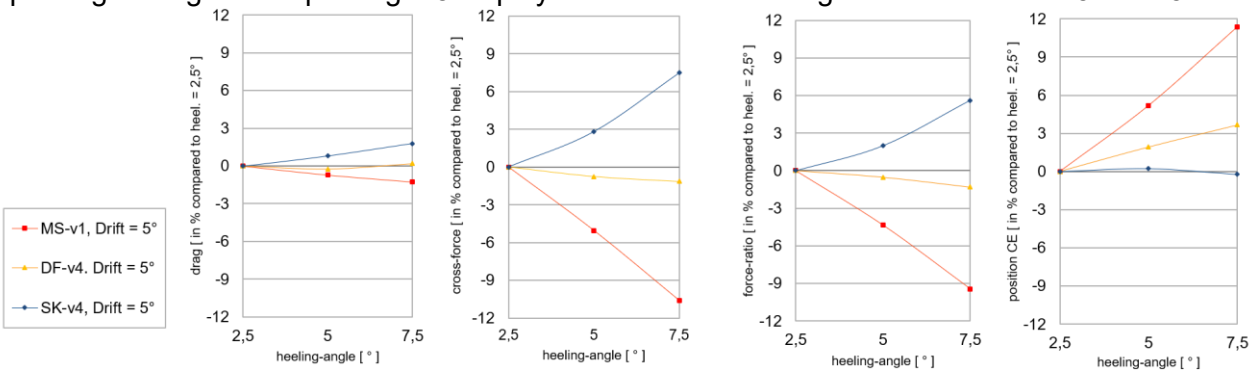

Figure 48. effect of heeling angle on drag, cross-force, force-ratio and the hydrodynamic center of effort.

While performance increases for SK-v4 (force-ratio increases, no change for the $C_{E,hydro}$), the opposite is true for the center-skeg variant. Force-ratio is reduced for CS-v1 by about 9% and the center of effort moves forward by more than 10%. For the double fin variant (DF-v4) the negative effects due to heeling are only small.

The different behavior due to heeling can be further explained by analyzing the pressure slices (Fig. 49) through the vector fields of the three different design variants.

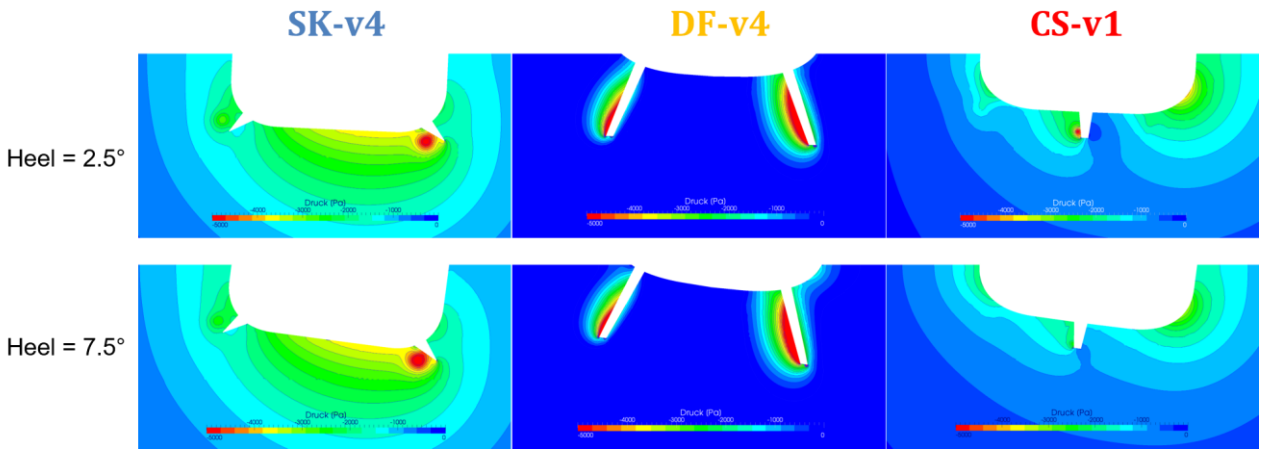

Figure 49. effect of heeling angle on performance, pressure slice.

For SK-v4 (on the left-hand side) increased heeling angles lead towards increased draft for the sideward positioned keel. The low-pressure core in the center of the vortex is slightly increased whereby the induced drag is increased as well. The opposite occurs for CS-v1 (righthand side). Effective draft of the centered keel is reduced. At the same time the bilge (with bilge-keel) moves down for increased heeling angles whereby inflow towards the center-skeg is disturbed. Resulting from this is the breakdown of the attached vortex at the center-skeg. The loss of cross-force at the center-skeg is the reason for the forward shifted center of effort and the reduced force-ratio. For variant DF-v4 (in the center of Fig. 49), a slight reduction of the pressure-field of the leeward (left) fin can be observed. This reduction is made good again by a performance increase for the luv-side fin (starboard) due to increased draft and a more vertical fin position.

3.4.7 Lessons Learnt

Three different appendage-design concepts have been discussed and analyzed in detail. In conclusion it can be stated that the conventional center-skeg design (CS-v1) shows major deficits as soon as the ship is subject to steady heeling angles. The double-fin variant (DF-v4) shows significantly higher performance values. Especially if the double fin would be realized as a double rudder configuration, the overall performance will likely be further increased. The limiting factor for the double fin or double rudder design with respect to the application large and powerful WPS, is the limited size of these rudders or fins. In case of double rudders, the higher costs need to be considered.

For primarily wind powered sailing ships, the most promising concept however is the delta-shaped side-keel configuration. This concept has the lowest initial drag values if designed moderately. Further, the side-keels can be combined with an efficient rudder configuration for increased vessel performance. The ‘Wagner-Keel’ concept is completely passive and thus it is cost-efficient and could also be retrofitted to almost any existing modern flat-bottom ship hull, perfectly adapted in size and longitudinal position to the requirements of the WPS.

4. RESEARCH FOR THE HYDRODYNAMIC LAYOUT OF JUREN-AE

In the framework of the project ‘Transition to Low Carbon Sea Transport’ (LCST), a bilateral research and development project between Germany and the Republic of the Marshall Islands (RMI), the University of Applied Sciences Emden-Leer (HEL) developed a concept design for a small primarily wind powered island supply vessel.

The passive but still efficient appendage design concept based on the delta-wing principle was chosen for further design investigations due to its perfect suitability for the anticipated task. The remoteness of the RMI trading area in the middle of the Pacific Ocean requires a solid and robust technology. Draft limitations due to the shallow entrances into the lagoons of the atolls, require a hull

and keel design with lowest possible draft. Retractable systems were considered unsafe, since the trading area is poorly charted. Often the vessels navigating the remote outer islands and atolls of RMI need to completely rely on echo sounding devices and often even a lookout is positioned at the bow of the vessels to detect uncharted reefs, while the ship enters or navigates inside the shallow lagoons.

In the framework of the design process for JUREN AE a series of towing tank measurements were carried out in order to identify the most suited hydrodynamic layout for the ship. The concept for the delta-shaped side-keels was investigated and compared towards two other possible solutions with the goal to verify and improve empiric analytical approximations that are used for vessel performance predictions.

4.1 Hydrodynamic Concept Design for the Sailing Vessel JUREN AE

The hydrodynamic layout for the sailing cargo vessel JUREN AE foresees medium sized delta shaped bilge-keels that are positioned aft of the mainframe of the vessel. These keels are expected to have several advantages compared to a centered keel. The sideward positioning will not increase the initial draft of the hull, but when the vessel is heeled the keels will become more and more effective the larger the heeling angle is, due to increasing effective draft. Compared to a centered keel system, this delta-shaped bilge-keel configuration can be smaller in size due to higher efficiency, thus also improving vessel performance in engine mode due to reduced frictional drag, as long as the alignment of the keels is following the streamlines of the hull.

As the JUREN AE is a primarily wind propelled sailing vessel, the hydrodynamic concept needs to be aligned to the aerodynamic design of the ship. Fig. 50 shows the concept design including approximate $C_{E,aero}$ for the sail-system and for hull and superstructure.

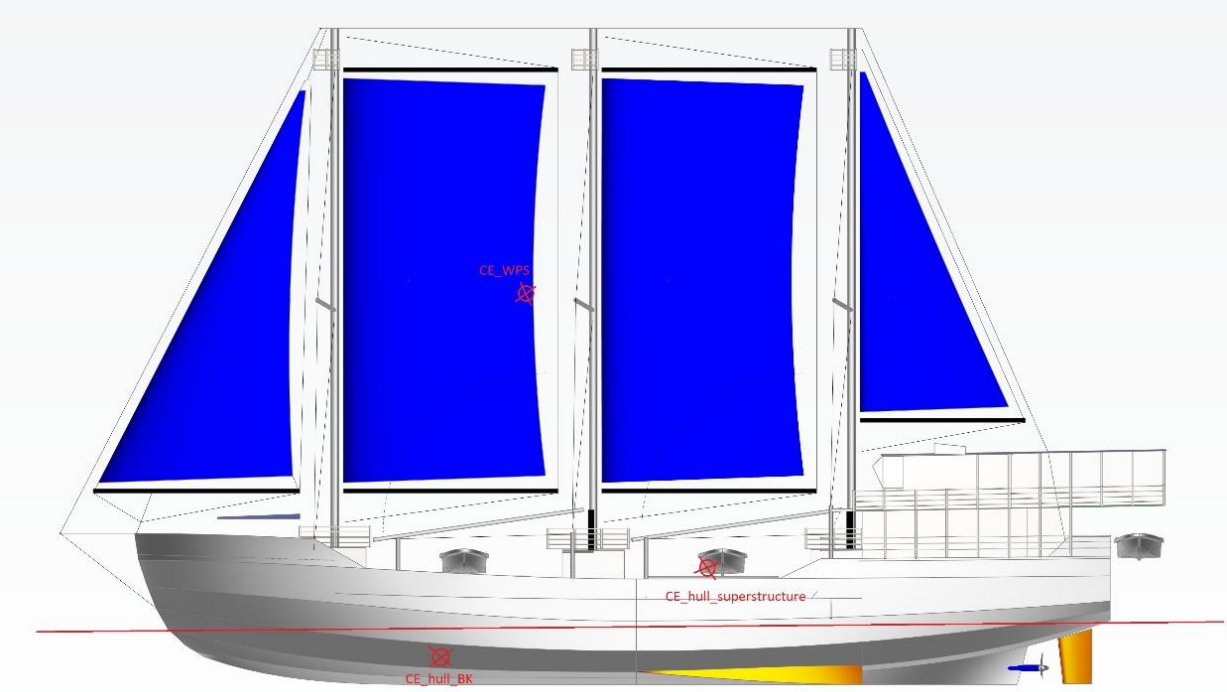

Figure 50. parametric 3D-Model used for initial design and calculations created within CAESES.

The hydrodynamic layout is designed with a strong focus on vessel safety against accidental groundings. Retractable dagger-board systems would be the most efficient solution (same as for racing yachts), in this case however they are excluded due to high risk of accidental damage.
Possible appendage systems are therefore the classical centered bar-keel, no keel (deadrise hull with center-skeg only) or the above discussed delta-shaped side-keels/bilge-keels (Wagner Keels). The centered single rudder is designed rather large in order to contribute to the required side force.

Additionally, the rudder needs to provide enough steering capacities even without the accelerated flow due to the propeller. Moreover, the recuperating propeller (extracting energy for hotel-load or charging of batteries) will further slow-down the approach velocity on the rudder, whereby the generated rudder forces are further reduced.

4.2 A modular Towing Tank Model for the RMI-Design

The modular scale model is fabricated by the use of 3D-Print technology, based on the existing numerical tender design model. Fig. 51 shows the center-skeg only version.

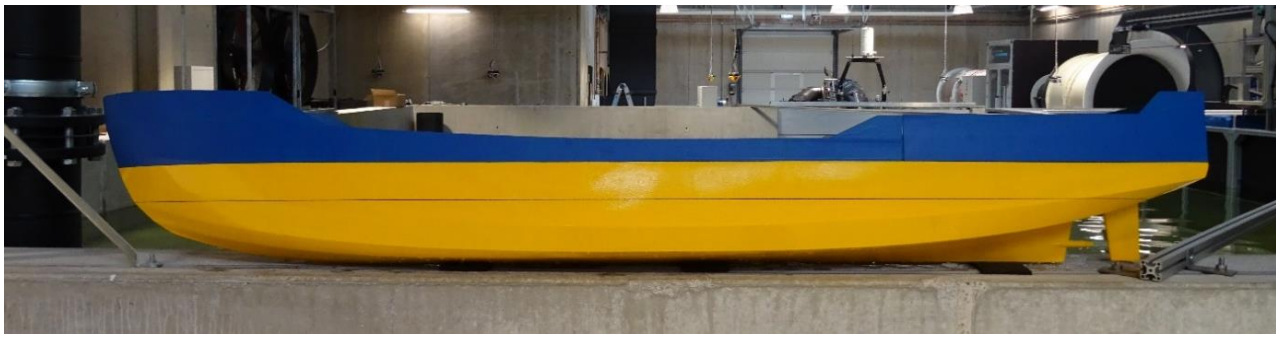

Figure 51. Towing-tank model with center-skeg and rudder, side-view.

Fig. 52 display the towing tank model with the bar-keel configuration (left) and the two delta-shaped bilge-keels (right).

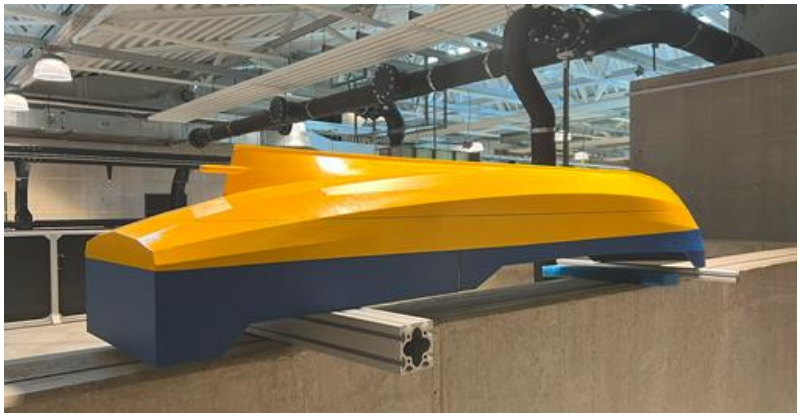

Figure 52. RMI-Design – towing-tank model with bar keel (left) and delta-shaped bilge-keels (right).

Data for added draft and surface areas for these two variants is given in Tab. 3. Turbulence stimulation is achieved by applying sand strips according to ITTC guidelines and recommendations.

Table 3. RMI-Design - appendage data.

	Additional surface area	Added draft	Keel length
Only center-skeg	0.0 m²	0.0 m	-
Bar-keel	14.0 m²	0.2 m	35.0 m
Delta-shaped bilge-keels	20.3 m²	0.0 m	11.0 m

4.3 Preparations for Towing-Tank Testing Series

Fig. 53 shows the placement of ballast within the model as well as the model guidance on the towing carriage. Below the yaw-angle adjustment unit, the 6-DOF sensory equipment (forces and torque moments) and the cardan joint towards the model can be seen as well.

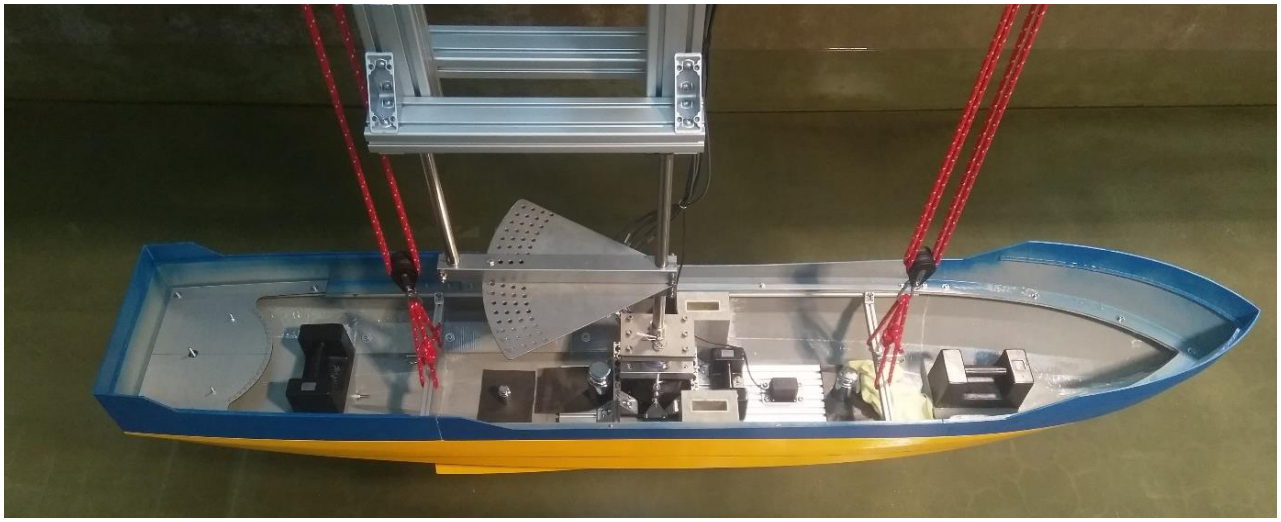

Figure 53. Placement of ballast inside the model.

The two pulleys, equipped with spring trolleys, were used to place the ballast in the model according to calculated weight distribution at the two attachment positions. Trim of the vessel was double-checked by measuring draft at FP and AP. An IMU-Unit is used to measure accelerations in all three axes as well as turning rates, allowing to document the actual floating position as well. The aim of the testing program is to provide input data that can be used within a performance/power prediction program tool (VPP, PPP). Relevant data in this context is:

- smooth water resistance curve: C_r, C_t, $1+k$
- hull-keel polar curves: C_{xyvh}, $C_{y,vh}$, $C_{xy,vh}$, $C_{E,hydro}$
- influence of rudder: validate/adapt analytical formulas, β_H-reduction factor

Smooth water resistance is done according to the ITTC recommendations. The form factor $(1+k)$ is measured for the bare hull without appendages. All measurements have been repeated three times and average values were calculated by using Fourier decomposition of the measured signals. Acceleration and jerk values were selected such that the initial bow-wave in the beginning of the run does not affect the measurement. The value cropping starts after all initial movements (especially around the y-axis, as a result from the initial acceleration) have faded. All series were measured in mixed order to detect systematic errors. For measurements including leeway angles, the measured angles under load were used for all calculations. The same accounts also for the carriage speed.

4.4 Smooth Water Towing Resistance

Towing resistance tests were done according to ITTC recommendations for vessel speeds from 3 kn (Froude number $Fn = 0.074$) to 17.4 kn ($Fn = 0.426$). Measurements were taken for the bare hull, excluding any appendages. Based on Prohaska Method the factor $1+k$, could be evaluated with 1.02. Very slow towing speeds for 3, 4, and 5 kn have been neglected for the linearization procedure.

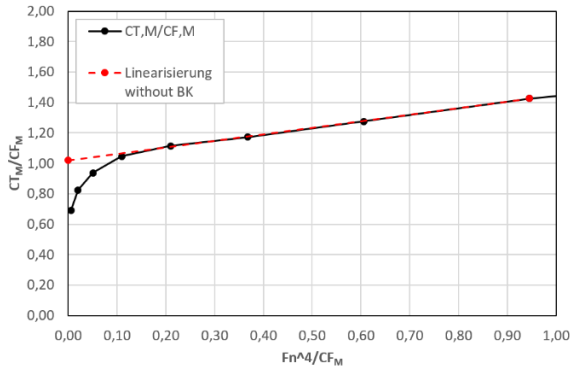

Figure 54. Linearization with Prohaska Method.

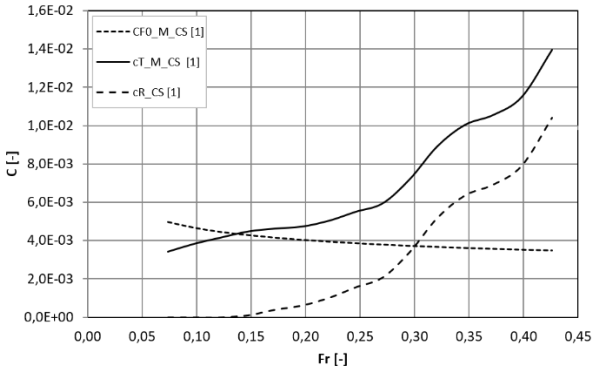

Figure 55. Towing resistance results in model-scale.

The model-scale towing resistance coefficients, shown in Fig. 55, show good values for Froude numbers up 0.28 which corresponds to a vessel speed of around 11 kn. Above that value a steep increase for the resistance coefficients can be observed.

Design speed for this vessel is 7 kn in engine mode and up to 12 kn using the INDOSAIL wind propulsion system. Predicted towing resistance for the full-scale vessel without appendages is displayed in Fig. 56 and Fig. 57. At engine design speed a total resistance R_t value of 7.37 kN is calculated. For the expected maximum sailing speed at 12 kn the total resistance value is around 45 kN.

The results for the smooth water towing resistance tests are, in the context of evaluating the efficiency of the appendage system, only relevant concerning the differences in initial drag (leeway angle of 0°) and are therefore not further discussed in this report. Differences concerning the initial drag values mainly result from added wetted surface area for the bilge-keel variant as well as for the bar-keel variant. The center-skeg only variant corresponds with the above tested variant 'bare hull without appendages'.

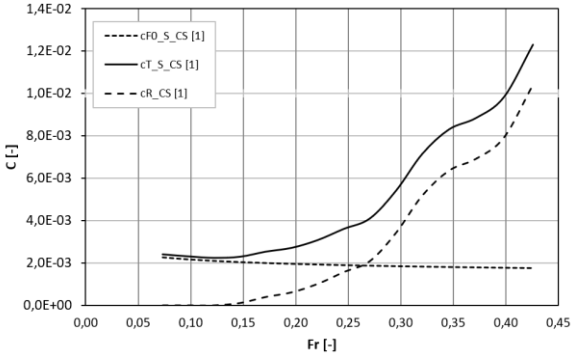

Figure 56. Coefficients for full scale prediction

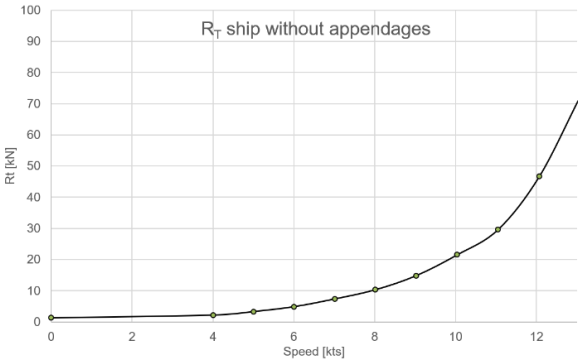

Figure 57. Prediction of towing resistance Rt for the bare hull without appendages

4.5 Hydrodynamic Polar Curves

The hull-keel polar curves are measured for a typical vessel speed (sailing with the WPS) of 9 kn. Since cross-force and induced drag is caused primarily by pressure differences, frictional components can be neglected whereby the measured coefficients ($C_{y,vh}$ and $C_{xy,vh}$) for the scaled model at a single (typical) speed are also valid for full scale predictions at varying vessel speeds.

The formulas used to determine the coefficients are:

$$c_{y,vh} = \frac{2\,F_{y,vh}}{\rho\,{V_h}^2\,S}, \tag{1}$$

and

$$c_{xy,vh} = \frac{2\,F_{xy,vh}}{\rho\,{V_h}^2\,S}. \tag{2}$$

The induced force component $F_{xy,vh}$ is the difference between the measurement including a varying yaw angle in the coordinate system of vessel motion (V_h) and the measurement at zero yaw angle. Fig. 58 shows the predicted cross-force ($F_{y,vh}$) and induced resistance values ($F_{xy,vh}$) for the three analysed keel design variants. The black dashed curve represents the results based on an analytical calculation (slender body theory) used for later performance calculations within the concept design process.

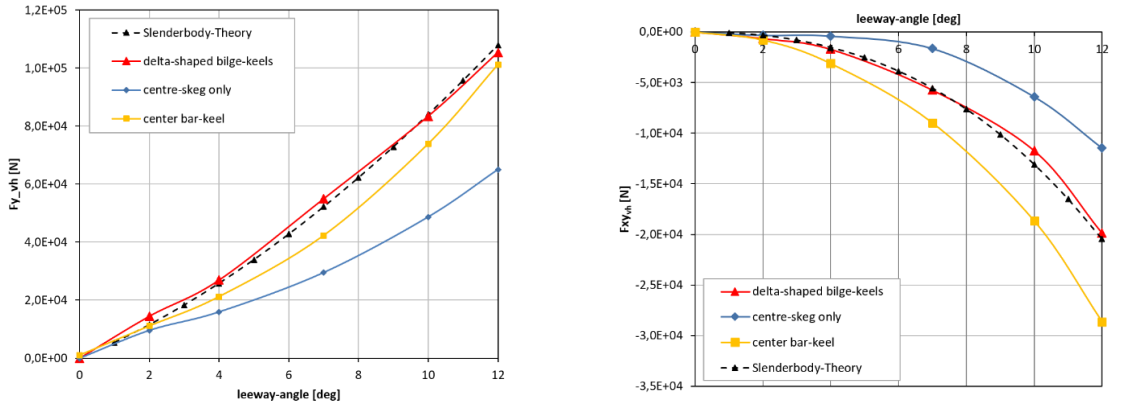

Figure 58. Cross-force ($F_{y,vh}$) and induced resistance ($F_{xy,vh}$) prognosis for full scale vessel.

The delta-shaped side-keel variant shows the highest cross-force values at moderate induced resistance. The bar-keel shows in this measurement series unexpected high induced resistance values. A clearer picture is given by the cross–force–drag curve. Initial drag is based on the above shown Rt calculation.

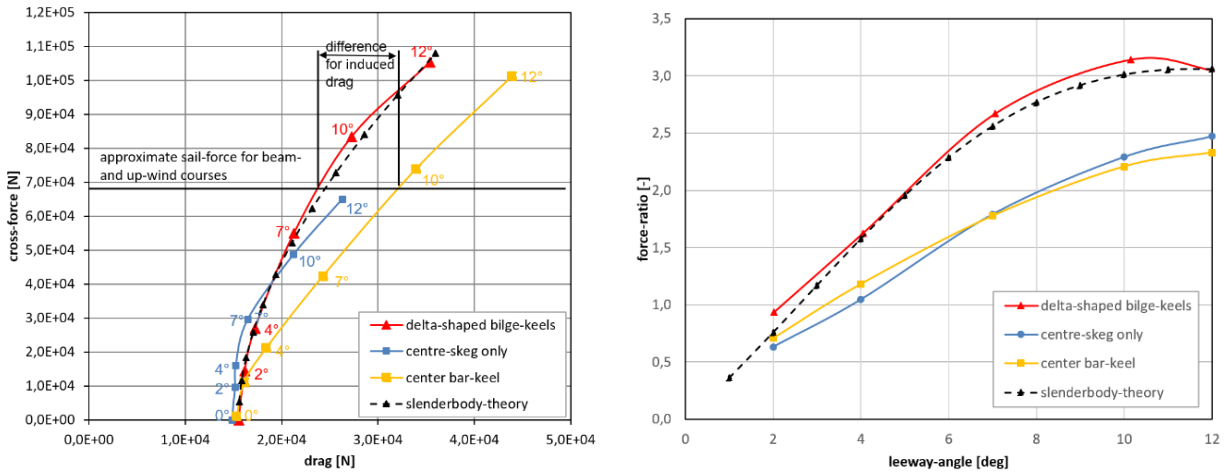

Figure 59. Cross-force-drag (left) and force-ratio (right) for full scale vessel without rudder.

For an approximated cross-force of 68 kN resulting from the INDOSAIL WPS at beam and upwind courses, the delta shaped bilge keel variant shows significantly reduced induced drag values at lower leeway-angles, leading to increased vessel performance. Force-ratio for the delta-shaped side-keels is increased by 20% to 30% for leeway angles in the relevant range of 5° to 10°compared to the two other design variants.

4.6 Hydrodynamic Center of Effort

The center of effort is the relevant information for a velocity prediction calculation to determine required rudder cross-force in order to equalize the yawing momentum. Fig. 60 shows the $C_{E,hydro}$ for the three keel concepts. The vertical axis shows measured hydrodynamic cross-force.

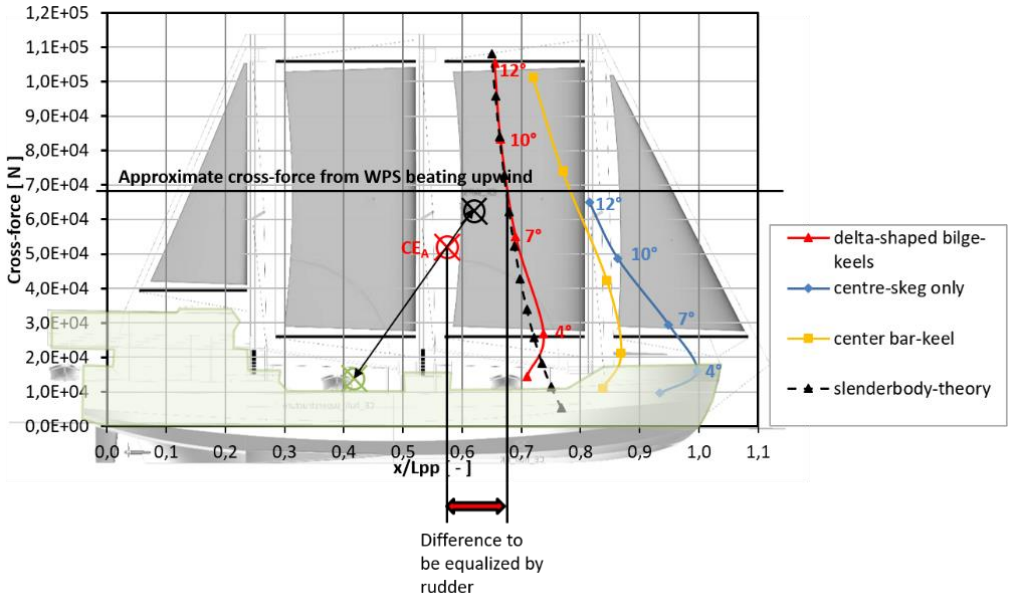

Figure 60. compare hydrodynamic center of effort to requirements from WPS.

The remaining offset that must be equalized by the rudder depends on the keel-variant. The side-keel concept results in favorable $C_{E,hydro}$ positions of about 10% forward of the $C_{E,aero}$ while the other two version need to equalize around 25% of L_{PP}.

4.7 Effect of Rudder on Sailing Performance

Rudder measurements were done for a leeway-angle of 7° and a heeling angle of also 7°. Rudder angles are varied from -20° to +20°. Important for the rudder calculations is the reduction of the inflow angle at the rudder position due to the appendage layout upstream. This factor is measured by identifying the rudder-angle of zero cross-force. For the RMI-design this factor is approximately 0.5. For the analytical rudder calculation, the flow speed reduction due to wake needs to be considered. Wake number is estimated with $w = 0.1$. The measured and calculated rudder cross-forces are given in Fig. 61.

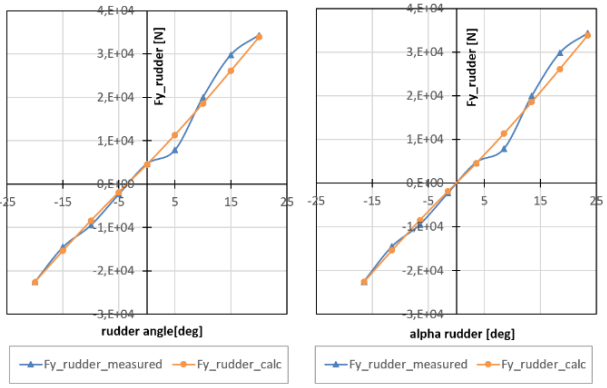

Figure 61. measured rudder cross-forces and analytical calculation.

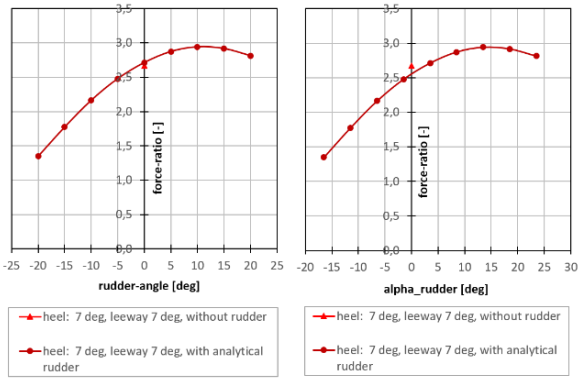

Figure 62. change of force-ratio due to added rudder forces.

Fig. 62 displays the change in force-ratio if the rudder is considered. Force-ratio is increasing due to the effects of the rudder for rudder angles of up to 10°. For higher rudder angles performance of the ship will be reduced again.

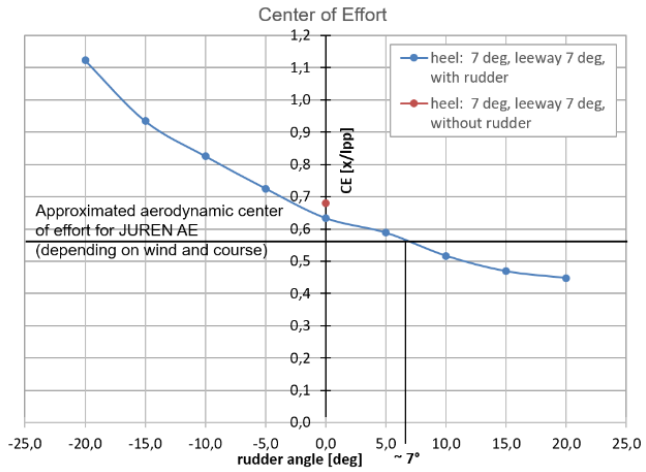

Figure 63. change of hydrodynamic center of effort due to rudder cross-force.

Figure 64. Model of JUREN-AE in towing-tank at Maritime Testing Facilities in Leer.

Fig. 63 displays the resulting change of the $C_{E,hydro}$ due to the rudder for the side-keel variant. The required position at around 57% of L_{PP} (aerodynamic center of effort) is reached with a rudder angle of about 7 degrees. This leaves enough room for manoeuvring the vessel before stall at the rudder occurs.

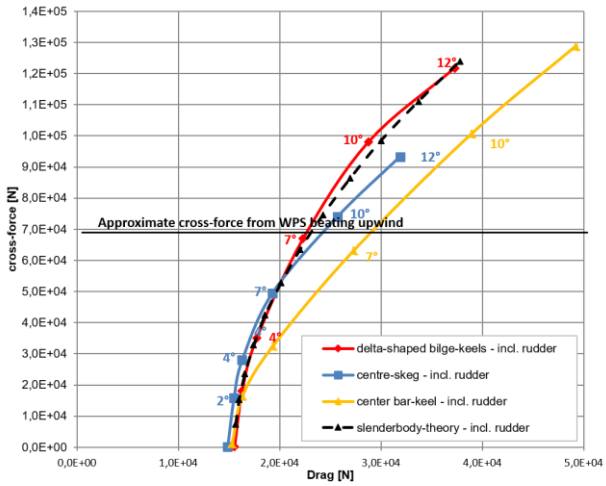

Figure 65. cross-force-drag curve including rudder and balanced yawing moment.

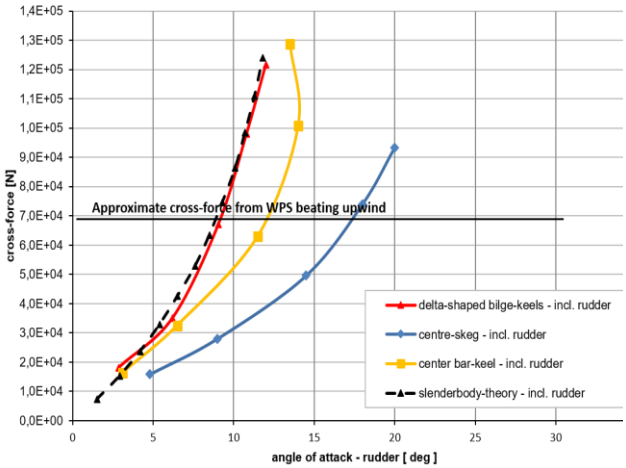

Figure 66. resulting angle of attack at rudder for equalized yawing moment.

If the analytical rudder is included, the difference between the center-skeg only variant towards the side-keel variant is much smaller. But looking at the angle of attack, that is required to balance the yawing moment, it becomes clear that the rudder is clearly overloaded for the center-skeg only variant (α ~17°). Also the resulting leeway angle is about 2° higher for the center-skeg only variant. Compared to the bar-keel variant a significant total drag reduction can be observed for leeway angles above two degrees.

4.8 First Preliminary Performance Results from JUREN-AE

Preliminary proof of concept is provided by the results of the sea-trials of JUREN AE conducted in May and June 2024 after the completion of the vessel in Korea. During these sea trials the standard procedure for measuring maneuvering capabilities and measuring vessel speed were done in nearly

perfect conditions (completely flat sea and no wind) in front of the shipyard AsiaShipbuilding in Geoje. Fig. 67 and Fig. 68 show the vessel just before launch (displaying the keels) and during the first sea-trials.

Figure 67. Delta-shaped keel at starboard side, Korea 2024.

Figure 68. JUREN AE during second sea-trial, Korea 2024.

The results of the sea-trials for JUREN AE are given in Fig. 69, displaying the maneuvering chart. The reached top speeds of about 9.66 kn is only slightly lower than the predicted speed of about 10.3 kn. This deviation from the predicted speed is likely the reduced engine RPM of only 1946 rpm instead of 2000 rpm as was anticipated during design-phase based on the towing-tank experiments for vessel resistance and the selected propeller and engine values. Further uncertainties in the predictive calculation are wake-number and thrust-deduction.

Very promising is the excellent maneuvering characteristics with turning circles of less than $3\,L_{PP}$. With respect to these relatively large keels maneuvering capabilities have been seen critical throughout the design phase by many observers. These first results prove that the concept of these keels works not only in theory but has proven itself also in a real application.

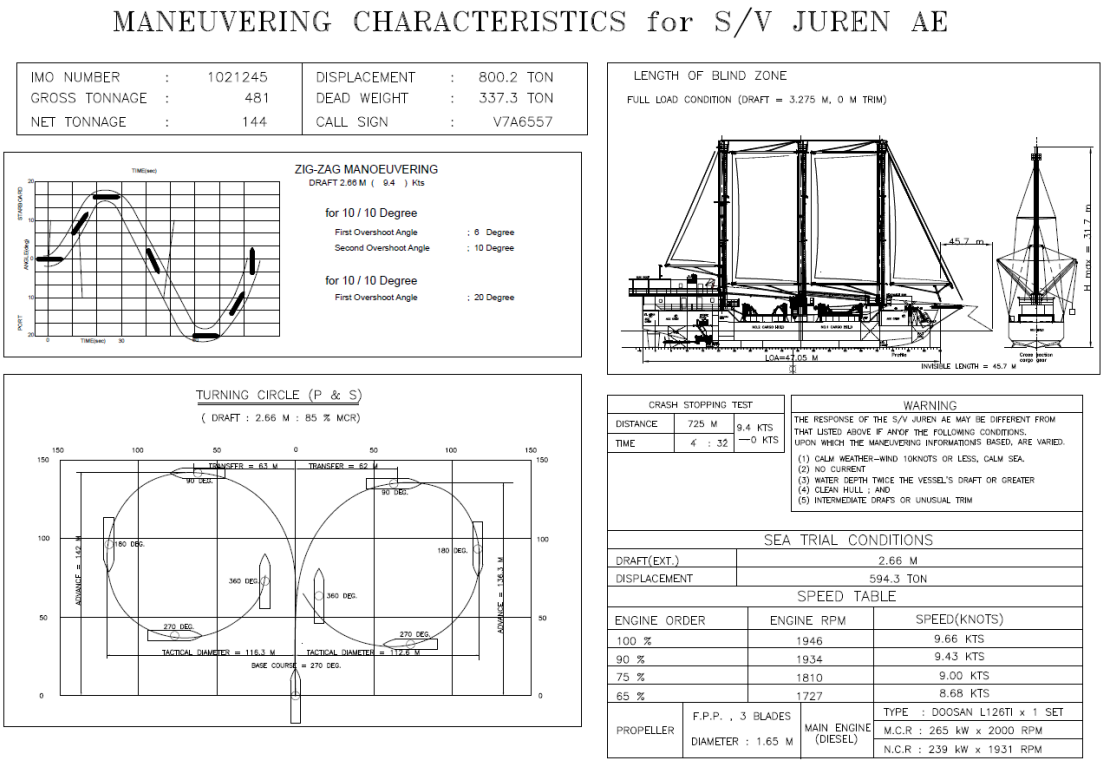

Figure 69. Manoeuvring Chart of JUREN AE.

Sailing capabilities of the vessel so far look very promising as well. The balancing of aero- and hydrodynamic forces works very well. Only small rudder angles of less than 3° are needed to keep JUREN-AE on track during sailing. Also tacking maneuvers look promising. During first sea trials under sails the vessel was able to tack even in very light wind conditions. The delivery voyage to RMI in July 2024 also revealed high potential with reached sailing speeds of more than 10 kn without engine support.

However, for a detailed performance analysis and evaluation of drag- and cross-forces as well as required rudder-angles also in recuperation mode at different courses sailed towards the wind, further tests are needed and will be done in the near future during operation in RMI.

4.9 Conclusion

The presented towing-tank analysis provides further insight into the capabilities of the design ideas of delta-shaped bilge-keels. In addition, towards the previous CFD study the results underline the potential of the concept especially compared to the traditional bar-keel design concept. However, the setting for the RMI-design differs from the previous study. The hull is designed with deadrise, leading towards a situation that offers good flow conditions also for a centered keel system (bilge of the ship is not blocking the flow around the centered bar-keel). Further the basic hull is designed for all variants with a center skeg that allows the installation of a simple single propeller drivetrain. Other than the 'bare hull without skeg' of the previous CFD study, this center skeg variant in combination with deadrise offers by itself a good design option since the resulting edge at the keel will already work as a reasonably good 'leeway reduction' feature. Additionally, this second study includes the positive influence of the rudder on total performance of the hydrodynamic layout. Since every rudder is designed for maximized cross-forces and minimized drag, the rudder usually offers higher force-ratios compared to the combined hull-keel system.

Compared to the centered bar-keel variant, the delta-shaped side-keels offer a clear advantage due to the lower induced drag values leading towards higher force-ratios, and better positioned center of effort due to the possibility of choosing the longitudinal position of the keels as required.

The center-skeg only variant relies in large parts on the efficient usage of the rudder, leading towards increased performance in comparison to the two other design options for small leeway angles. The reason for this is the lower wetted surface area (no additional keels) resulting naturally in less initial drag. However, the higher load on the already comparatively large rudder, leads to much higher required rudder angles. This high rudder load will be even increased if the propeller, positioned in front of the rudder, is used for energy recuperation. The large wind-milling propeller will further slow-down inflow speed on the rudder and thus likely would lead to a breakdown of the rudder forces due to stall during maneuvering. Since the ability for recuperation is a crucial energy concept feature for the design of JUREN-AE (it is expected that recuperation in combination with PV-capabilities will provide enough power for covering the hotel load) this variant yields a high risk for the energy efficient operation of the vessel.

For the hydrodynamic design of JUREN-AE, the concept of 'Wagner Keels' thus promises clear advantages compared towards the alternative design variants. Based on these findings the size of the two side-keels for JUREN AE are reduced by about 20% compared to the initial design discussed above (towing tank analysis) in order to decrease initial drag by reducing the wetted surface area of the keels and further to increase the positive influence of the rudder on total performance.

5. OUTLOOK

With the delta-shaped bilge-keels (Wagner-Keels), aimed at maximizing vortex-lift effects, a highly efficient and flexible keel system for handling large side-forces induced by a major wind-propulsion system, has been discovered. The system can be used for very different modern hull shapes and can also be retrofitted to most flat-bottom hulls. Major benefit is its cost efficient and passive design

that does not increase the draft of the vessel as well as the flexibility of the concept concerning size and positioning of the keels in line with the specific requirements of the ship design. Necessary for good performance is the alignment towards calculated streamlines in order to minimize initial drag and prevent the forming of vortexes and additional drag at zero leeway angle when the vessel is sailing downwind or in engine mode.

The implementation of the concept for the JUREN AE revealed high potential so far. Manoeuvring of the ship in engine mode was not compromised by the large keels and the sailing abilities of the vessel revealed an astoundingly good performance. Further performance tests onboard JUREN AE will be conducted in the near future.

The keel concept will be part of further comparison studies within our current wind-ship design projects at University of Applied Sciences Emden-Leer focusing again on larger hull designs as well as different drive-train layouts and rudder configurations.

Based on the investigations and findings on the concept of Wagner-Keels, it is expected that this concept can be transferred to almost any kind of vessel, independent from vessel size. Even if wind propulsion is not part of the design task it can be expected that based on these findings standard bilge-keels used only for roll-damping will perform better if they are designed as 'Wagner-Keels' based on the 'vortex-lift' principle with a delta shaped planform, due to lower frictional resistance and increased force-ratios.

ACKNOWLEDGEMENTS

The initial research at TUHH in 2011 and 2015 was supported by Prof. Thomas Rung (TUHH) and Dipl.-Ing. Peter Schenzle (scientist and expert for sailing ship theory). Research on the concept design and towing-tank measurements for JUREN-AE were done within the framework of the R&D project 'Transition to low carbon sea transport' (LCST), coordinated by Emden/Leer University of Applied Sciences, managed by 'Deutsche Gesellschaft für Internationale Zusammenarbeit (GIZ) and funded through the International Climate Initiative (IKI) of the German Government.

REFERENCES

Bradbury, W.M.S. (1985). An Experimental Investigation of the Flow Past Hulls at Leeway. *Journal of Wind Engineering and Industrial Aerodynamics* 20(1-3), pp. 227-265, https://doi.org/10.1016/0167-6105(85)90020-0

Dykstra Naval Architects (2013). The Ecoliner Concept. *Dykstra Naval Architects*, January 29th 2013, URL: https://www.dykstra-na.nl/designs/wasp-ecoliner/

Ferziger, J. H., and Peric, M. (2008). Numerische Strömungsmechanik. *Springer Verlag*, https://doi.org/10.1007/978-3-540-68228-8

Luckering, J. M. (2019). The Discovery and Prediction of Vortex Flow Aerodynamics. *The Aeronautical Journal* 123(264), pp. 729-804. https://doi.org/10.1017/aer.2019.43

Marchaj, C. A. (1986). Seaworthiness - The Forgotten Factor. *International Marine Publishing Company*, ISBN 9780877422273.

Marchaj, C. A. (2003). Sail Performance: Techniques to Maximise Sail Power (revised edition). *Adlard Coles Nautical*, ISBN 978-0071413107 / 0071413103 .

Irkal, M. A. R., Nallayarasu, S., Bhattacharyya, S.K. (2016). CFD Approach to Roll Damping of Ship with Bilge Keel with Experimental Validation. *Applied Ocean Research*, 55, pp. 1-17. https://doi.org/10.1016/j.apor.2015.11.008

Polhamus, E. (1966). A Concept of the Vortex-Lift of Sharp-Edge Delta Wings based on a leading-edge-suction analogy. *NASA*, URL: https://ntrs.nasa.gov/citations/19670003842

Schenzle, P. (2010). Technik und Strömungsmechanik von Segelschiffen. Lecture notes, Hamburg University of Technology.

Van der Kolk, N. (2020). Sailing Efficiency and Course Keeping Ability of Wind Assisted Ships (dissertation), TU-Delft. https://doi.org/10.4233/uuid:8707309f-b9a3-4e09-916d-8fb64328a138

Van der Kolk, N. and Jacobi, G. (2024). Comprehensive Assessment of Bilge Keels and Fins for Enhancing Wind Powered Vessel Performance: Bridging Laboratory Insights to Operational Efficiency. *RINA Wind Propulsion 2024* Conference, London, UK.

Wagner, B. (1967). Windkanalversuche für einen sechsmastigen Segler nach Prölss. *Schriftenreihe Schiffbau,* 173. https://doi.org/10.15480/882.614

Wagner, B. (1967). Fahrtgeschwindigkeitsberechnung für Segelschiffe. *Schriftenreihe Schiffbau,* 132. https://doi.org/10.15480/882.588

Wagner, B. (1968). Schrägschleppversuche für einen Seglerrumpf mit und ohne Balkenkiel und für den „Mariner“. Schriftenreihe Schiffbau, 186. https://doi.org/10.15480/882.622

Wagner, S. (2011). Hydrodynamische Analyse und Vergleich zweier Langkiel-Segelyachten. *Hamburg University of Technology.*

Wagner, S. (2015). Hydrodynamische Analyse Zur Querkraftentwicklung An Fracht-segelschiffsrümpfen. *Hamburg University of Technology.*

Yasukawa, H., Hirata, N. and Yamazaki, Y. (2017). Effect of Bilge Keels on Maneuverability of a Fine Ship. *Journal of Marine Science and Technology*, 23, pp. 302–318, https://doi.org/10.1007/s00773-017-0474-6